

## Chapter 5

# Timing Noise Analysis of 16 pulsars

### 5.1 Rotational Irregularities of Pulsars

Long-term timing observations have shown that the rotation rates of pulsars are subject to two types of irregularities: continuous erratic fluctuations known as "Timing Noise" and sudden discrete jumps in rotational frequency, mostly positive, known as "Glitches". While glitches are seen in very few pulsars, most of the relatively young pulsars show some degree of timing noise. Both these types of irregularities are predominantly seen in younger pulsars. For example, two relatively young pulsars namely the Crab and the Vela pulsar, are well known for their high level of intrinsic timing noise and frequent glitches.

This section gives a brief review of these phenomena, namely the Glitches and the Timing Noise. In section 2, we have described the analysis procedure we have used to examine the data on 16 pulsars for Timing Noise. Results of the timing noise analysis done using *strength parameter* calculations are presented in section 3 of this chapter.

#### 5.1.1 Glitches

Glitches have been observed so far in  $\sim 20$  pulsars or so (Lyne et al., 1994). These are characterised by sudden changes in the rotational frequency ( $\nu$ ) and simultaneous changes in the frequency derivative ( $\dot{\nu}$ ) of the pulsar. The fractional change in the rotational frequency ( $\Delta\nu/\nu$ ) is of the order of  $10^{-9}$  to  $10^{-6}$ , while the fractional change in the frequency derivative ( $\Delta\dot{\nu}/\dot{\nu}$ ) is seen to vary widely from 0.1% to 10%. Very young pulsars such as the Crab have shown small glitches with fractional change in the period of the order of  $10^{-9}$  (Lyne et al. 1993), while the adolescent pulsars such as Vela, whose age is of the order of  $10^4$  yrs, show large glitches with  $\frac{\Delta\nu}{\nu} \approx$  a few  $\times 10^{-6}$  once every few years (Alpar et al. 1993). The glitch is followed by a relatively slow exponential recovery of the rotation frequency and frequency derivative towards their preglitch values. This "postglitch relaxation" takes places over a period of days to years.

The post-glitch behaviour differs considerably from one pulsar to another, i.e. the rate at which frequency derivative decays to pre-glitch value varies widely for different pulsars.

For example, in Vela pulsar about half of the initial increment in  $\dot{\nu}$  decays away in a matter of days, followed by a slow relaxation of the remainder of the increment (McCulloch et al. 1987, 1990, Cordes et al. 1988, Alpar et al. 1993). In PSR B0355+54, almost all of the frequency derivative rise has been seen to decay away within a time scale of 44 days, possibly leaving a permanent step only in the rotation frequency (Lyne 1987). On the other hand, the glitches in the Crab pulsar show a persistent and cumulative increase in the frequency derivative (Lyne et al. 1993) which means that this pulsar is slowing down faster than it would have without the glitches. Some pulsars do not show any relaxation at all, which indicates either that the relaxation time is so long that the relaxation is not obvious or that the relaxation time is very short and the timing observations are too sparse to notice the relaxation.

There are two aspects of glitches which need to be explained: (1) a sudden jump in  $\nu$ ,  $\dot{\nu}$  and (2) postglitch relaxation. Many models have been proposed to explain one or both of these aspects of glitches, for example the heat pulse, starquake, **two-component** (refers to crust and core) and vortex creep models. Of all the models **proposed** so far, the theory of vortex creep has been successful to some extent in explaining especially the post-glitch relaxation.

One of the earliest models proposed was the Starquake Model by Ruderman (1969). He suggested that a starquake might arise due to the change in the ellipticity of the crust of the neutron star as it slows down. The oblateness of an equilibrium spheroid will decrease as the rotation rate decreases. Hence, as the neutron star slows down, stresses steadily build up in the crust until they reach a point where the crust cracks and readjusts to a less oblate form. This reduces the moment of inertia  $I$  and due to conservation of angular momentum the star will spin-up, which will be seen as a glitch. The change in rotation angular frequency  $\Omega$  can be given approximately in **terms** of the change in oblateness  $\epsilon$ :

$$\frac{\Delta\Omega}{\Omega} = -\Delta\epsilon = -\frac{\Delta I}{I} \quad (5.1)$$

This **model** can explain the glitch itself, but cannot account for postglitch relaxation. For the Crab pulsar  $\Delta\epsilon = -10^{-7}$  every 10 years and the current value of  $\epsilon$  is about  $10^{-3}$ . Clearly the time scale on which  $\epsilon$  will decay due to the glitch activity is much greater than the age of the pulsar and this is quite satisfactory. However for the Vela pulsar  $\Delta\epsilon = -2 \times 10^{-6}$  every 3 years and  $\epsilon = 10^{-4}$ . In this case  $\epsilon$  would disappear in only about 100 years which is only 1% of the age of the pulsar (Pines, **Shaham & Ruderman** 1972). The current rate of glitching in the Vela pulsar cannot be sustained, and another source of the discrete spin-ups is necessary.

**Baym et al.(1969)** proposed a 'two-component model to explain the relaxation **after** the first Vela glitch. In this model, the neutron star consists of a **charged, non-superfluid** crust and a neutron superfluid interior which is loosely coupled to the crust. They assumed that the initial speed-up is produced by **starquake** and in that case, this simple model gives rise to the "glitch-function" which describes the exponential recovery:  $\Delta\nu(t) = \Delta\nu_0 \times [1 - Q(1 - e^{-t/\tau})]$ . Here  $\Delta\nu_0$  is the initial rotational frequency increase and  $Q$  is the **fraction** which recovers on a **timescale**  $\tau$ . However, this **model** couldn't explain the second

exponential recovery seen in the 5th Vela glitch (McCulloch et al. 1983). Further this model is also found to be inconsistent with the persistent shift in the frequency derivative following the 1975 glitch in the Crab pulsar and the glitch in PSR B0525+21 (Downs 1982).

Models proposed later involved an explanation in terms of interactions between the neutron star crust and the superfluid neutrons. A quantitative explanation was presented in terms of the pinning and unpinning of microscopic **vortices** within the neutron star. The area density of vortices is a measure of the rotation rate of the superfluid. Hence, the spin-down of the superfluid requires that the vortices move radially outward from the spin **axis**. This is believed to take place in the superfluid core of neutron stars, which comprises the bulk of the moment of inertia of the star. This component is predicted to be tightly coupled to the crust, via interactions of the population of the core protons and electrons with the crust. It is the small component ( $\sim 1\%$  of the total **mass**) of the superfluid coexisting with the inner crust nuclei that is believed to be **responsible** for glitches. Anderson & Itoh (1975) pointed out that the crustal **superfluid** vortices may become pinned to the crustal nuclei **as** a result of attractive or repulsive interactions in this region of the neutron star. These pinned vortices cannot move outwards and hence the angular velocity of **the** crustal **superfluid**,  $\Omega_s$ , will **remain** constant. Thus, a **differential** velocity will be developed between the two components **as** the angular velocity of the crust,  $\Omega_c$ , decreases. This difference in rotation rates will give **rise** to a radial force, popularly known as **Magnus** force which will exert force on the vortices radially outwards. Once the difference in angular velocity attains a critical value, there will be a sudden catastrophic unpinning of vortices and subsequently these vortices will **flow** outward causing an increase in the angular momentum of the crust and this is what observed as a glitch.

Alpar et al. (1984a,b) have greatly extended these basic ideas into their theory of vortex creep. This theory attempts to explain both the **process** that **causes** glitches and the postglitch relaxation on the basis that there exist a number of distinct superfluid regions in the inner crust with different pinning energies. The vortex creep model **has** been successful in explaining the postglitch behaviour of some pulsars, particularly the Vela pulsar (Alpar et al. 1993). In fact, Alpar et al. (1994) have proposed that the **small** glitches in young pulsars are caused by **starquakes**. As a pulsar **ages** and cools down, the thermal creep rate is not **sufficient** to relieve the **stresses**, resulting in large glitches such as those observed in the Vela **pulsar**. In old pulsars, the slow-down rate is small, **so** the **stresses** take much longer to build up to a critical point, resulting in very infrequent glitches.

Observations of glitches provide an important avenue for studying the structure and dynamics of neutron stars. It remains a great challenge for both observers and theoreticians to account for the diversity of **postglitch** behaviour **observed** in pulsars and, **as** a result, to provide further **insights** into neutron star interiors,

### 5.1.2 Timing Noise

Timing noise is characterised by a continuous, unpredictable, phase wandering of the pulses relative to a simple slow-down model. The characterisation of timing noise is an important step towards gaining a better understanding of neutron star dynamics. It is seen most predominantly in the Crab and other pulsars with large period derivatives (Cordes and Helfand 1980). Millisecond pulsars exhibit very little timing noise and consequently have received considerable attention in this regard (Blandford et al. 1984, Ryba & Taylor 1991, Kaspi et al. 1994 and references therein). More than one physical processes may be responsible for the timing activity resulting from a time-varying component of the torque acting on the neutron star crust. There are two possible sources of such a torque: (1) an *internal* torque that may stem from the coupling between the crust and the superfluid interior of the neutron stars, as in the case of glitches, and (2) an *external* torque related to the pulsar magnetosphere (the "radiation torque").

Timing Noise was first recognized by Boynton et al.(1972), who examined the first two years of timing data from the Crab pulsar. **Quasi-sinusoidal** structure present in the residuals over the span of a few months led them to **conclude that** a noise process **was** responsible for the observed behaviour. They were the first to suggest that the rotational irregularities might arise from a simple random walk process comprising of small steps in one of three **observables** - the pulse phase  $\phi$ , frequency  $\nu$  or frequency derivative  $\dot{\nu}$ . The random walks in  $\phi$ ,  $\nu$  and  $\dot{\nu}$  can **be** explained by random changes in the emission region or beam direction, moment of inertia of the star and the process of rotational energy **loss** respectively. The Crab pulsar timing noise was found to be consistent with a random walk in the **pulse** frequency (Boynton et al. 1972, Groth 1975). A **similar** analysis by Cordes & Helfand (1980) showed that the timing noise of a number of other pulsars could also be described by a simple random walk process.

**Cordes & Downs** (1985) later investigated the timing noise in a sample of 24 pulsars. They found that the timing activity is highly correlated with period derivative but not with **pulsar** period. Their analysis shows **that** the timing activity in some pulsars cannot be modelled in terms of idealised, large rate random walks. Instead, the activity is due to discrete events in one or more of the timing parameters, possibly superimposed on an idealised random walk process, or a mixture of such processes. **Unlike** glitches, these discrete events have been found to exhibit both positive and negative changes in  $\nu$  and  $\dot{\nu}$ . For example, Vela pulsar shows such microglitches with fractional magnitudes of  $|\Delta\nu/\nu| \leq 10^{-9}$  and  $|\Delta\dot{\nu}/\dot{\nu}| \leq 10^{-4}$ . **Cordes et al.(1988)** found that **these** events can have positive or negative step changes and that they occur roughly once every 100 days in Vela pulsar.

Also, some pulsars show some quasi-periodicities in their residuals which **may arise** due to **some** non-random causes of timing noise, such as (i) **oscillations** of the vortex lattice in the rotating superfluid; (ii) free precession of the neutron star; (iii) the presence of an **orbiting** companion and (iv) an **unusually** high value of  $\ddot{\nu}$ , that may be due to the long-term **linear** recovery in  $\dot{\nu}$  **from a past** glitch. The **timing** activity of only a few pulsars has been **associated with such non-random** causes.

## Proposed theories for Pulsar Timing Noise

A number of theories have been proposed to explain the underlying cause of timing noise. The theories can be classified as those relating to internal torque fluctuations and those that are external to the neutron star.

### Internal Torque Fluctuations

Soon after the starquake hypothesis, Pines & **Shaham** (1972) proposed *microquakes* to explain the random variation of **residuals**. Their assumption is that the neutron star rotation axis makes an angle  $\theta_0$  with an elastic reference **axis**. The component of the radiation torque perpendicular to the rotation **axis** may increase the misalignment and hence the crustal stress increases. These stresses tend to be **localised** and gives rise to *microquakes*, whereas the more global *macroquakes* are induced by a decrease in the stellar oblateness  $\epsilon$ , which appear as *glitches*. The timing noise can be due to a small number of "large" *microquakes*, such as the discrete events observed in some pulsars, or a large number of "**small**" *microquakes*, such as the stochastic models involving idealised random walk processes.

**Anderson & Itoh** (1975) suggested that, in addition to crustquakes, the restless **be-**haviour of pulsars could be due to the random pinning and unpinning of vortex lines as they creep outward through the crustal lattice. Hence, the slowing down of the **super-**fluid and the crust proceeds in an irregular fashion and is observed as timing noise in the rotation rate of the pulsar.

Lamb et al. (1978a,b) extended the work of **Anderson & Itoh** (1975) by proposing that random internal pinning and unpinning of vortices causes jumps in the angular momentum (steps in  $\Omega$ ) and produces a substantial torque on the crust which can be described in terms of a random noise process. Two basic types of events were considered, namely microglitches occurring as small *pulses* or, alternatively, as small *steps* in the angular velocity  $\Omega$ , of the crust. These basic events can be represented mathematically as

$$\Delta\Omega_c(t) = \sum_i \Delta\phi_i \delta(t - t_i) \quad (5.2)$$

and

$$\Delta\Omega_c(t) = \sum_i \Delta\Omega_i \theta(t - t_i) \quad (5.3)$$

where  $\delta(t)$  and  $\theta(t)$  are the delta and unit'step functions, and  $\Delta\phi_i = \Delta\Omega_i \delta t_i$  in terms of the size  $\Omega_i$  and duration  $\delta t_i$  of the  $i$ th event (Lamb 1981). These **processes** can produce the "phase noise" and "frequency noise" as considered by Boynton et al. (1972).

Greenstein (1979a,b, 1981) has suggested that timing noise arises from the dynamical response of a neutron star to a *heat pulse*. The model is based on the two assumptions: (i) the superfluid interior of a neutron star rotates more rapidly than the crust, and (ii) the frictional coupling between the superfluid and the crust increases with temperature. In this model, a sudden pulse of heat **causes** a sudden increase in the frictional coupling

which is then observed either **as** a glitch or slower variations that can be termed as timing noise. **With this model**, Greenstein predicted the internal temperature to lie between 2 and 4 million Kelvin, with individual events occurring no more than once every year. The internal temperature estimates translate into surface temperatures lying between  $3 \times 10^4$  K and  $4 \times 10^5$  K, depending on the mass of the star.

By studying the timing noise processes in isolated pulsars, Cordes & Greenstein (1981) considered eight mechanisms to account for the observed phenomenon. These were: (1) a continuous and erratic quaking of the crust or core of the star; (2) the random pinning and unpinning of vortex lines as they migrate through the crust ("hard superfluidity"); (3) accretion from the interstellar medium; (4) the sudden annihilation of vortex lines at the outer boundary of the superfluid; (5) pulse-shape changes; (6) the response of the superfluid interior to a continuous and erratic series of heat pulses; (7) the unpinning of vortex lines via crust breaking; or (8) external torque fluctuations related to the luminosity of the star. Each physical model was evaluated by comparing the noise strength expected from such a mechanism with the estimates obtained from the observations.

Cordes & Greenstein found the first five of these mechanisms to be too severely constrained to be considered as plausible causes for timing noise. In each case, the predicted noise strengths were found to be too small or too large, often by several **orders of magnitude**, and in some cases the mechanism is not able to produce **all** three types of simple random walk processes. On the other hand, mechanism 5 & 6 are capable of producing the observed strengths of random walk phenomena such as phase noise (PN) - random walk in pulse phase  $\phi$  and frequency noise (FN) - random walk in frequency  $\nu$ , but cannot readily explain the slow-down noise (SN) - random walk in **frequency derivative**  $\dot{\nu}$ .

Using the vortex creep theory, Alpar et al. (1986) constructed model noise power spectra for three different types of events that might **give** rise to timing noise. These are: (i) "pure" vortex unpinning events (**i.e** the scaled down versions of the large glitches), (ii) a process which is accompanied by vortex pinning (**e.g.**, breaking of the **crustal** lattice by pinned vortices), and (iii) "**external**" events that do not involve vortex unpinning. In order to test the three models, Alpar et al. examined the observational power spectra in  $\dot{\Omega}$  for 25 pulsars resulting from the work of Boynton & Deeter (1986). From this, they concluded that timing noise is probably due to physical processes in regions external to the weak **and** superweak pinning regions of the crustal **superfluid** that are thought to be responsible for glitches.

The **most** recent theory of pulsar timing noise has been proposed by Jones (1990). The theory is based on the existence of separate regions of pinned and corotating superfluid vortices within the neutron star, which have also been used to explain the postglitch relaxation in some pulsars. In this model, the cylindrical **surfaces** dividing the **regions have** time-averaged radii which may show secular change as the pulsar rotation rate decreases. Microjumps in the rotation frequency **and** frequency derivative with both positive and negative magnitudes, **as** found by Cordes & Downs (1985), are **caused by** transitions **between pinned** and corotating vortex states which produce small movements of the surfaces. This model **has** made considerable progress towards explaining the **nature** and variety of

microjumps observed in pulsars.

### External Torque Fluctuations

Cheng (1987a,b 1989) has developed a detailed model of pulsar timing noise in terms of magnetospheric fluctuations. He first investigated the pulsar timing noise in the context of the outer magnetospheric gap model of emission ~~from~~ fast-spinning pulsars, with particular reference to the Crab pulsar. According to this, pair production processes in the outer gap can give rise to fluctuations which result in rapid variation of the braking torque, and hence the stellar rotation frequency. The **time-scale** of the fluctuations is expected to be short ( $\sim 10$  ms), resulting in a series of  **$\delta$ -function-like** fluctuations in the braking torque. These fluctuations in the torque will produce a random walk in the rotation frequency (FN) with a strength parameter given approximately by

$$S_{\text{FN}} = \frac{\Omega}{8\pi^2} \left( \frac{I_{\text{tot}}}{I_c} \right)^2 \left( \frac{\delta N_{\mathbf{J} \times \mathbf{B}}}{N_{\text{tot}}} \right)^2 \frac{1}{t_{\text{age}}^2}. \quad (5.4)$$

where  $t_{\text{age}} = -\Omega/2\dot{\Omega}$  (the characteristic age of the pulsar),  $\mathbf{I}$ , and  $I_{\text{tot}}$  correspond to the **crystal** and total moments of inertia, and  $\delta N_{\mathbf{J} \times \mathbf{B}}$  is the fluctuation in the braking torque, based on the assumption that  $N_{\mathbf{J} \times \mathbf{B}}$  is the dominant stellar slow-down torque so that  $N_{\mathbf{J} \times \mathbf{B}} \approx N_{\text{tot}} = I_{\text{tot}}\dot{\Omega}$ . The squared fractional variation in the current braking torque is estimated to be approximately 0.1 for rapidly spinning **pulsars** and about ten times larger for slowly spinning pulsars (Cheng 1987a).

To explain the random walk in  $\dot{\Omega}$ , Cheng (1987b) proposed another magnetospheric model. This model is applicable to pulsars with a steady current flow in the outer magnetosphere, **e.g.**, the Vela pulsar. In such cases, the braking torque is perturbed by **microglitches** in the rotation rate of the neutron star, where he assumed that microglitches are produced by small-scale superfluid unpinning events **as** considered by Alpar et al. (1986). The perturbed torque remains unchanged until the next microglitch and hence the rate of torque variations is the same as the rate of **microglitches**. These step like changes in the torque give rise to a random **walk** in  $\dot{\Omega}$ , described by

$$S_{\text{SN}} = R(\Delta\dot{\Omega}_c)^2 = \frac{R}{4\pi^2} \frac{\Omega_c^2}{4t_{\text{age}}^2} \left( \frac{\delta N_{\mathbf{J} \times \mathbf{B}}}{N_{\mathbf{J} \times \mathbf{B}}} \right)^2 \left( \frac{N_{\mathbf{J} \times \mathbf{B}}}{N_{\text{tot}}} \right)^2 \quad (5.5)$$

where  $R$  is the rate of magnetospheric noise and the fractional fluctuation in the current braking torque is **an** unknown function which depends upon the detailed responding mechanism of the magnetosphere to the **microglitches** (Cheng 1987b).

Harding et al. (1990) have tried to see whether a chaotic **dynamical process** is responsible for the origin of timing noise. They applied the popular "**correlation sum**" technique which allows the "fractal dimension" of the system to be estimated. A low dimension is suggestive of a chaotic process. Harding et al. obtained a dimension of 1.5, suggesting that nonlinear dynamics may be the cause of timing noise in the Vela pulsar. However, when a similar analysis was performed on simulated random walk data, they also obtained

low fractal dimensions. They concluded that the correlation sum estimator for dimension is unable to distinguish between *chaotic* and *random* processes.

The study of pulsar timing noise is an important probe of the structure and dynamics of neutron stars. While a number of theories have been proposed, for example, involving crustquakes, heat pulses, superfluid vortex unpinning, **superfluid** rotation and external torque fluctuations, or a combination of such mechanisms, the origin of timing noise is still uncertain. None of the models explain *all* of the timing activity observed in the limited sample of pulsars investigated. Long-term timing observations of a much larger **sample** of pulsars are needed in order to gain a better understanding of **this** phenomenon. In the following sections, we present timing noise analysis carried out on our set of 16 pulsars using *strength* parameter *analysis*.

## 5.2 Timing Noise Analysis Procedure

The timing activity **as** outlined in the previous section may be a manifestation of the response of the neutron star to a *noisy* component of the torque acting on the crust. This noisy torque could arise from variations involving the moment of inertia or the magnetosphere of the neutron star. The timing residuals of some pulsars shows consistency with simple random process, while **residuals** of some more pulsars can be understood if one invokes a small number of resolved jumps in  $\nu$  and  $\dot{\nu}$ . The other sources of timing residuals are

- Quasi-periodic oscillations: Long term recovery in  $\dot{\nu}$  after a glitch will produce phase residuals that display a single cycle across the data span and a third order fit will result in a large measured **value** of the frequency second derivative  $\ddot{\nu}$ . This value and **the** corresponding "anomalous" braking index is always larger than the  $\ddot{\nu}$  and index due to the pulsar braking torque. But, there is no way of distinguishing between a glitch-induced and, for example, a random walk induced cubic term. Also the oscillations of the vortex lattice in the neutron superfluid may be excited under certain circumstances, **e.g.**, as a result of a glitch (Ruderman 1970a). These oscillations can produce a periodic wobble in the timing residuals of pulsars.
- Ruderman (1970b) suggested that free precession of the rotation axis of the neutron star may cause the small amplitude 'wobble' observed in the arrival times from **the** Crab pulsar. The instantaneous spin axis of an isolated star can precess if this **axis** **does** not coincide with the symmetry axis due to, for example, a non-spherical shape. This may cause a cyclical change in  $\alpha$ , **and** since the magnetic dipole radiation model predicts  $\dot{\nu} \propto \sin^2 \alpha$ , this will change the torque in a cyclical fashion and may be detectable in the timing data of **pulsars** (Cordes 1993).
- Presence of planets around neutron stars have **also been** proposed for the periodic variation seen in the timing residuals. Discovery of two planets around PSR

**B1257+12** (Wolszczan & Frail 1992, **Wolszczan** 1993,1994) is one example of such a case.

Considering the range of characteristic ages of pulsars in our sample, we don't expect to see any significant timing noise. Nevertheless, we examined the data to see if there are any interesting deviations in some cases, so that such objects can be studied in detail in future observations. With this in mind, we proceed with the timing noise analysis in this chapter. In our observational data of 16 pulsars, we do not detect any resolved jump either in  $\nu$  or  $\dot{\nu}$  over one and a half year span. So we made an attempt to **see** whether the noise seen in the residuals is consistent with a simple random walk **process**. We have carried out a Strength **Parameter** analysis, for which the procedure used is explained in this section.

As already mentioned, Boynton et al. (1972) were the first to suggest that rotational irregularities might arise from a simple random walk process comprising small step functions in one of three observables - the pulse phase  $\phi$  (**phase** noise, PN), frequency  $\nu$  (**frequency** noise, FN) or frequency derivative,  $\dot{\nu}$  (slowing-down noise, SN). The Crab pulsar timing noise was found to be consistent with a random walk in the pulse frequency (Boynton et al. 1972, Groth **1975b**). A similar analysis by Cordes & **Helfand** (1980) showed that the timing noise of a number of other pulsars could also be described by a simple random process.

The definition of a random walk process is as follows: A random walk in the kth derivative of the phase ( $\phi$ ) is defined as (Groth **1975a**)

$$\frac{d^k \phi(t)}{dt^k} = \sum_j a_j H(t - t_j) \quad (5.6)$$

where  $a_j$  is the amplitude j-th step occurring at a time  $t_j$  and H is a unit step function. The amplitudes are assumed to be random with zero mean. The random **walks** for  $k = 0,1,2$  correspond to PN, FN, SN respectively. A simulation of each of these random walk process is shown in fig(5.1). This simulation was performed as follows. A **gaussian** random noise of unit variance was generated with the **spacing** of one day between the points. Then these random noise is integrated to obtain phase which undergoes random walk with a rate of 1 per day. For frequency noise, once again the phase noise data was integrated. Another integration of the **above** data would give the simulated slowing-down noise data. At each stage, after integration, mean subtraction and **normalisation** was carried out, because **we** are interested only in the structure of the variation but not the absolute magnitude. The simulated data is shown in figure(5.1).

The random walk processes described above can be characterised by their second moments. To see whether such processes are responsible for the observed timing fluctuations, the estimated variances of the pulsar timing residuals is compared with the variance expected for a random **walk**. The timing noise variance is estimated as

$$\sigma_{\text{TN}}^2 = \sigma_{\text{R}}^2 - \sigma_{\text{W}}^2 \quad (5.7)$$

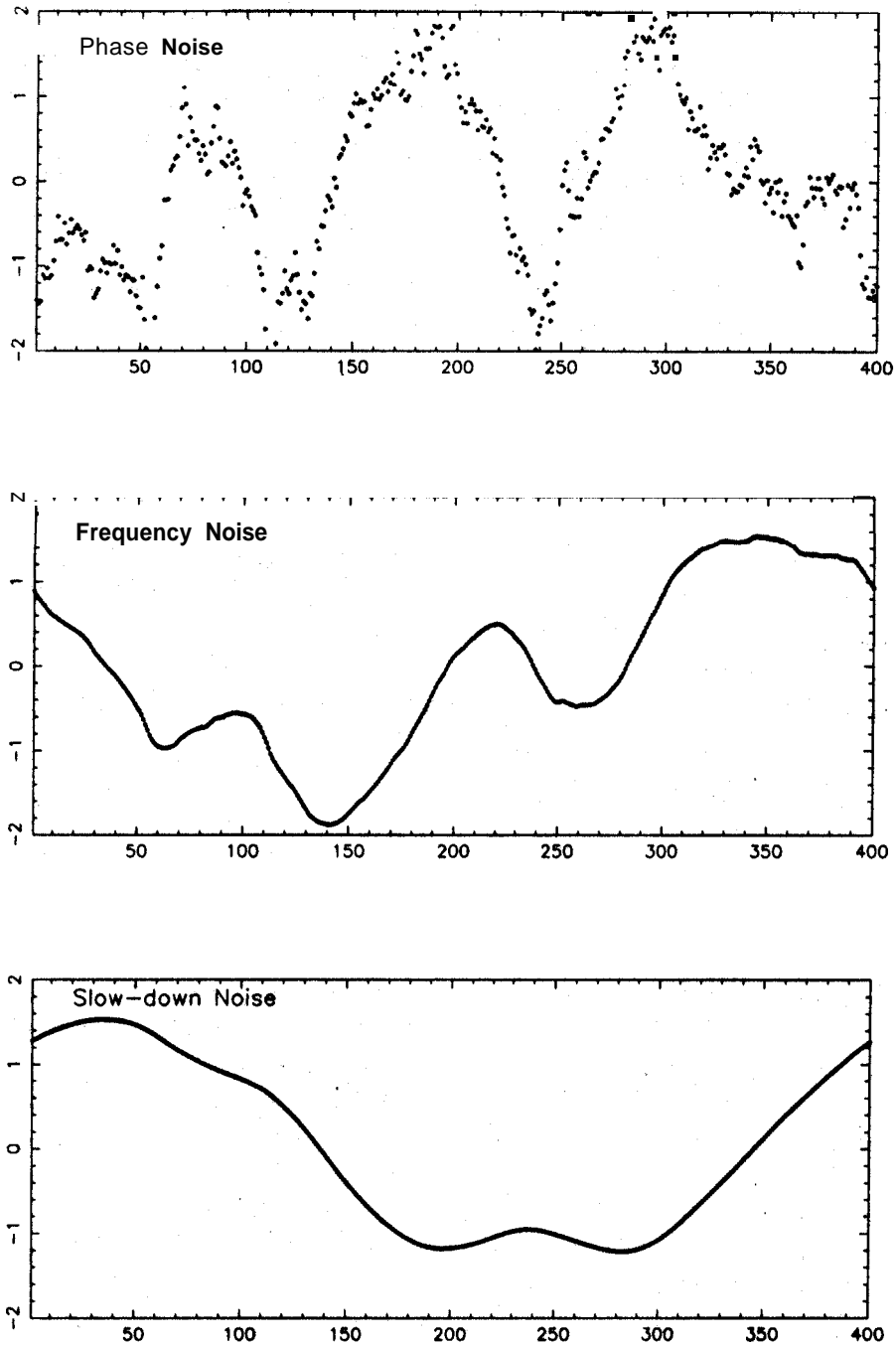


**Figure 5.1:** Simulation of Phase noise, Frequency noise and Slow-down noise over 400 days. Number of days is along x-axis and the amplitude is along the y-axis in arbitrary units.

---

where  $\sigma_R^2 = \sigma_R^2(m, T)$  is the mean square residual from an  $m$ -th order polynomial fit over a data span of  $T$  and

$$\sigma_W^2 = \sigma_M^2 + \sigma_J^2 \quad (5.8)$$

where  $\sigma_M^2$  is the mean-square white noise contribution from the measurement uncertainty and  $\sigma_J^2$  is the contribution due to the phase errors produced by pulse jitter which is estimated as (Hankins & Rickett 1975),

$$\sigma_J = \sqrt{\frac{w_s w_p P}{t_{\text{int}}}} \quad (5.9)$$

where  $w_p$  and  $w_s$  are the profile and **subpulse** widths respectively,  $P$  is the pulse period and  $t_{\text{int}}$  is the integration time. The **pulse** widths that we have used are estimated as discussed in the fourth chapter. Typical estimates of the sub-pulse width lie in the range 2 – 5 degrees of longitude (Taylor et al. 1975). Also, Taylor et al. have fitted a function for the observed pulse width of 18 pulsars and obtained an expression as

$$w_s = 0.01 P^{0.5} \quad (5.10)$$

where  $w_s$  and  $P$  are in seconds. Measurement noise will dominate the white noise for weak pulsars, whereas the pulse jitter tend to dominate **for** stronger ones. In our case, we found the measurement uncertainty ( $\sim 0.3$  mP) is much less than the spread seen in the phase residuals ( $\sim$  few mP). **This** would be due to **excess** pulse jitter which can be explained as follows. The telescope **used** for our observation is sensitive to only one **polarisation** which will introduce additional apparent pulse jitter along with the intrinsic one **as** the observed pulse shape of the polarized component depends upon the time of observation in a day because of the **Faraday** rotation due to the ionosphere. Our daily observation is mostly confined within an hour or **so**, and hence when seen over days to months the spread is quite large compared that within a day. Because of these reasons, we have estimated the  $\sigma_W$  from the data itself by finding the **rms** of successive differences of the phase residuals and dividing it by  $\sqrt{2}$ . Then the true timing noise contribution ( $\sigma_{\text{TN}}$ ) to the phase residuals was estimated by quadratic subtraction of the white-noise estimate from the measured **rms** phase residual, as given in eqn(5.7).

The random walks have second moments that are characterised by the **strength** parameters,  $S_k$ , where

$$S_0 = R \langle (\Delta\phi)^2 \rangle, \quad S_1 = R \langle (\Delta\nu)^2 \rangle, \quad S_2 = R \langle (\Delta\dot{\nu})^2 \rangle \quad (5.11)$$

(Cordes & Greenstein 1981). The  $\langle \rangle$  denote an ensemble average and  $\Delta\phi$ ,  $\Delta\nu$  &  $\Delta\dot{\nu}$  are the small steps in the rotation variables which occur with an average rate  $R$ . The strength parameters can be estimated from the **rms** residual,  $\Delta_{\text{TN}}(m, T)$ , after performing a least squares polynomial fit of order ' $m$ ' over a data span  $T$ . Following Cordes(1980),

$$S_k = C_{k,m}^2 \left[ \frac{\sigma_{\text{TN}}^2(m, T)}{\langle \sigma_{\text{RW}}^2(T) \rangle_u} \right] S_u \quad (5.12)$$

where  $C_{k,m}$  is the correction factor that compensates for the fraction of the timing noise variance absorbed by the polynomial fit and  $\langle \sigma_{\text{RW}}^2(T) \rangle_u$  is the ensemble average second moment for a random walk of unit strength ( $S_u=1$ ). In the ideal case of uniform sampling, equation 5.12 becomes

$$S_0 = 2C_{0,m}^2 \sigma_{\text{TN}}^2(m, T) T^{-1} \quad (5.13)$$

$$S_1 = 12C_{1,m}^2 \sigma_{\text{TN}}^2(m, T) T^{-3} \quad (5.14)$$

$$S_2 = 120C_{2,m}^2 \sigma_{\text{TN}}^2(m, T) T^{-5} \quad (5.15)$$

for phase noise(PN), frequency noise(FN) and slowing-down noise(SN) respectively. The magnitude of the correction factor increases with the order of the random walk because an m-th order polynomial absorbs a larger fraction of the SN variance than the FN or PN variance. The correction factors also depend on the order of the polynomial used to fit the data. Using random walk simulations, Cordes (1980) found these factors to be:  $C_{0,2} \approx 3.7$ ,  $C_{1,2} \approx 15.5$ ,  $C_{2,2} \approx 23.7$ , and  $C_{0,3} \approx 4.1$ ,  $C_{1,3} \approx 27.3$ ,  $C_{2,3} \approx 71.1$ .

Consistency of one of the noise processes with the pulsar data is indicated if  $S_k$  is found to be independent of T and if the constraint  $RT > 1$  is satisfied (Cordes & Downs 1985), which can be measured using the statistic

$$F = \frac{S(T_{\text{max}})}{S(T_{\text{min}})} \quad (5.16)$$

where  $T_{\text{max}}$  and  $T_{\text{min}}$  are the maximum and minimum time spans from which the strength parameter estimates can be obtained. If the data are consistent with a pure random walk process,  $F \approx 1$ , otherwise F will be a strong function of  $T_{\text{max}}/T_{\text{min}}$ .

If  $S(T_{\text{max}})$  and  $S(T_{\text{min}})$  are statistically independent (derived from non-overlapping data spans) and have a Gaussian distribution, then  $\log F$  will also have a Gaussian distribution with a standard deviation (Cordes & Downs 1985)

$$\sigma_{\log F} = \sigma_{\log S} \left( 1 + \frac{1}{N_{\text{min}}} \right)^{\frac{1}{2}} \quad (5.17)$$

where  $N_{\text{min}}$  is the number of independent strength estimates used to estimate  $S(T_{\text{min}})$ . But if the number of points used to estimate S itself is not very large, then the above formula has to be modified as follows:

$$\sigma_{\log F}^2 = \sigma_{\log S}^2 \left( \frac{1}{N_{\text{min}}} \right) \left( 1 + \frac{1}{N_{\text{dof}}^{\text{min}}} \right) + \sigma_{\log S}^2 \left( 1 + \frac{1}{N_{\text{dof}}^{\text{max}}} \right) \quad (5.18)$$

where  $N_{\text{dof}}^{\text{max}}$  and  $N_{\text{dof}}^{\text{min}}$  are the number of independent points used to estimate the strength parameters for the maximum and minimum time spans respectively. In our analysis,  $N_{\text{min}} = 2$  and typical values for  $N_{\text{dof}}^{\text{max}}$  and  $N_{\text{dof}}^{\text{min}}$  are 7 & 2 respectively. This gives an typical error bars on  $\log F$  to be 0.38 for PN, 0.7 for FN and 0.9 for SN. The values of  $\sigma_{\log S}$  are estimated from 500 simulated realisations of random walks by D'Alessandro (1995) as  $\approx 0.21, 0.40$  and  $0.50$  for  $k = 0, 1, 2$  random walks respectively.

### 5.3 Results and Discussion

The phase residuals exists for 16 pulsars spanning over an year, sampled roughly at **monthly** intervals with one more data set at 6 months apart. We have used only the first one year of data for timing noise analysis to ensure near-uniform sampling. And the last data set is used to refine our position estimates, because any sinusoidal timing noise present would have been absorbed in our earlier position fitting done with one year data as explained in fourth chapter.

Before any analysis was performed, the residuals **were** averaged over a day for all the pulsars, by finding the mean epoch and the mean residual within the day. The averaging is done to reduce the spread of the residuals due to the measurement uncertainty, since we are interested only in the slower variation of the residuals in the timescale of a year. The averaged phase residuals of all the 16 pulsars after second-order/third-order fit is shown in fig(5.2) and fig(5.3).

The error on the daily-averages of the phase residual is calculated as

$$\sigma_{ave,j} = \frac{\sqrt{\sum_i (\phi_{i,j} - \phi_{ave,j})^2}}{N_{ave,j}} \quad (5.19)$$

where  $\phi_{i,j}$  is the individual phase residual,  $\phi_{ave,j}$  is the mean phase residual in the  $j^{\text{th}}$  day and  $N_{ave,j}$  is the number of points averaged within that day. Since, we see the spread quite large compared to the  $\sigma_{ave,j}$ , the **rms** white noise ( $\sigma_w$ ) for the whole set is calculated as follows:

$$\phi_{dif} = \phi_{ave,j+1} - \phi_{ave,j} \quad (5.20)$$

$$\sigma_w = \sqrt{\frac{\sum_{j=1}^{(N_{tot}-1)} (\phi_{dif} - \bar{\phi}_{dif})^2}{2(N_{tot} - 1)}} \quad (5.21)$$

where  $\phi_{dif}$  is the successive differences of the averaged phase residuals,  $\bar{\phi}_{dif}$  is the mean of the above differences and  $N_{tot}$  is the total number of averaged phase residuals available. The points which showed excessive deviation (compared to that expected, **i.e.** deviation  $\gtrsim 3\sigma$ ) in the difference residuals are neglected in this estimation.

Strength parameters and their ratios were estimated for each of the random walk processes as explained in the section 5.2. The estimates were obtained by considering one year as the maximum time span and  $\sim 6$  months as the minimum time span. Hence, we have two blocks of data to calculate  $S(T_{min})$  and the averaged value of this is used to calculate the ratios. Second order polynomial fits were used separately for both the minimum blocks and the maximum to obtain the **rms** timing noise for the strength parameter computations. For almost all the pulsars second order fits were sufficient, and we see very insignificant variation between the second and third order fits. The analysis results are presented in Table (6.1). Column (1) gives the pulsar name, followed by the period of the pulsar in column (2) and the **logarithm** of the characteristic age in column (3). Columns (4) & (5) lists the **maximum and minimum** data span. Column (6) and (7) lists the rms white noise

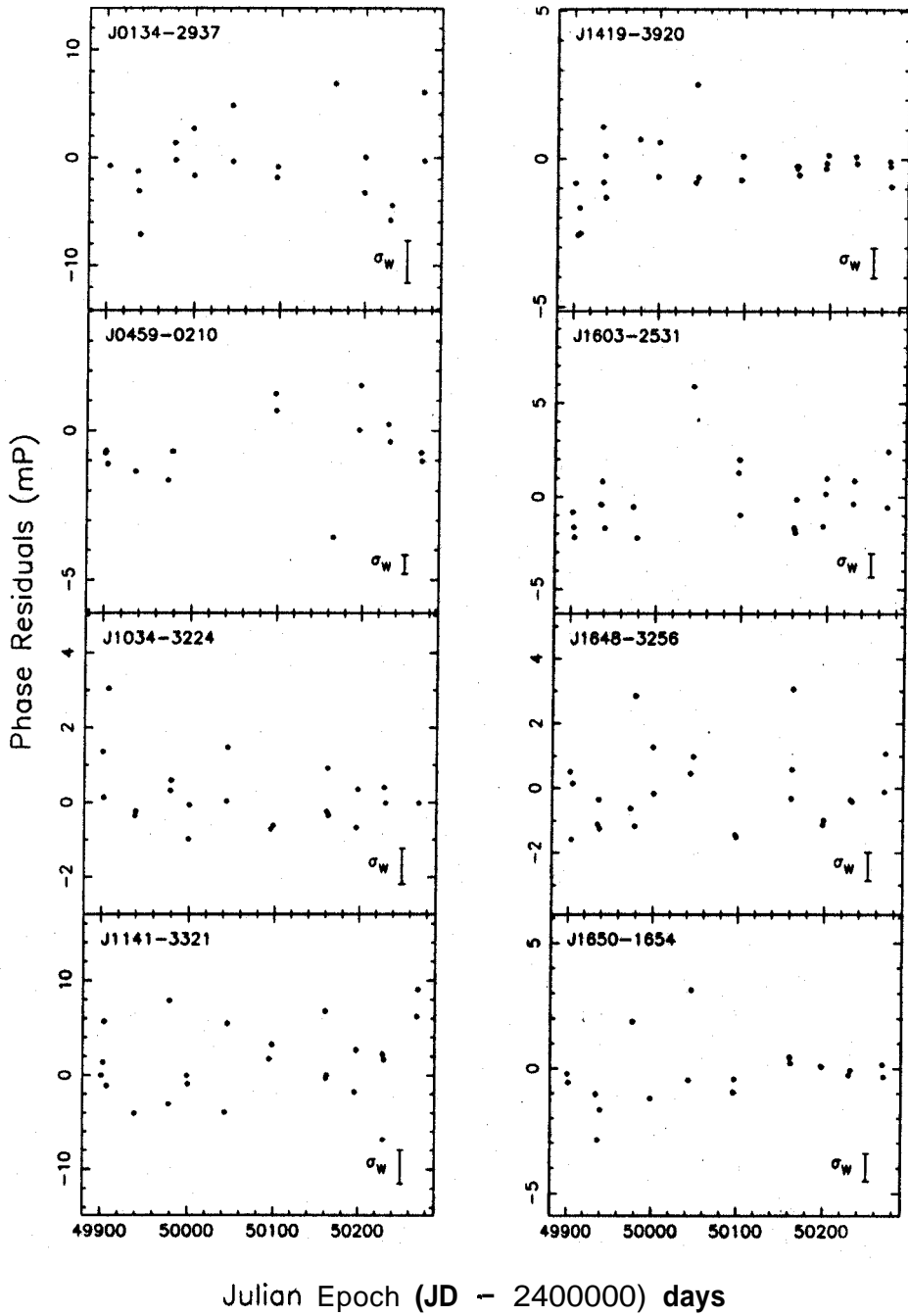


Figure 5.2: Averaged phase residuals for 8 pulsars.

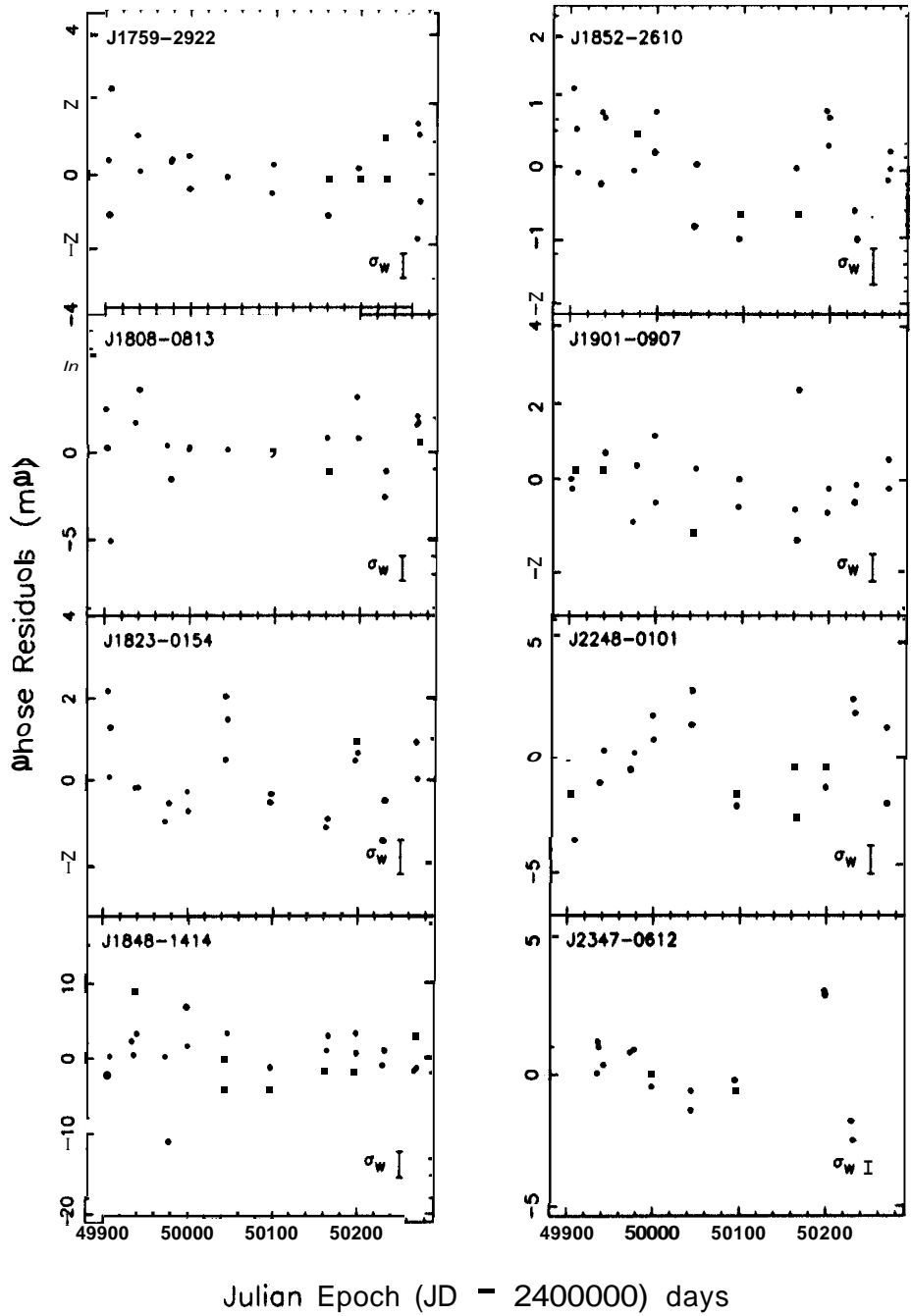


Figure 5.3: Averaged phase residuals for 8 pulsars.

Pulsar Name (J2000)	Period (secs)	Age (log $\tau$ )	Data Span		oR (mP)	oW (mP)	$\sigma_R/\sigma_W$	Ratios		
			T <sub>max</sub> (days)	T <sub>min</sub> (days)				log (F <sub>PN</sub> )	log (F <sub>FN</sub> )	log (F <sub>SN</sub> )
<b>J0134-2937</b>	0.136962	7.4	366	157	3.59	3.92	0.9			
50459-0210	1.133076	7.1	369	150	1.25	0.63	2.0	-0.25	-1.35	-2.44
J10343224	1.150590	7.9	367	159	0.87	0.96	0.9			
51141-3321	0.145734	7.0	369	160	3.93	3.53	1.1	-0.28	-1.10	-2.92
514143920	1.096806	7.3	369	160	1.03	1.01	<b>1.0</b>	-1.88	-2.70	-3.51
<b>J1603-2531</b>	0.283070	6.5	368	158	1.31	1.26	<b>1.0</b>			
51648-3256	0.719455	6.5	368	158	1.23	0.88	1.4	-0.24	-0.98	-1.72
<b>J1650-1654</b>	1.749552	6.8	369	160	1.22	1.10	1.1	-0.88	-1.70	-2.52
51759-2922	0.574399	6.3	367	158	0.95	0.67	1.4	-0.38	-1.13	-1.89
51808-0813	0.876044	7.1	370	159	1.43	1.39	<b>1.0</b>			
51823-0154	0.759777	7.0	367	159	0.99	0.81	1.2			
51848-1414	0.297769	9.0	367	159	3.70	3.30	1.1			
51852-2610	0.336337	7.0	367	159	0.61	0.53	1.2	0.33	-0.35	-1.03
<b>J1901-0907</b>	0.890964	7.8	367	159	0.81	0.65	1.3	-0.30	-0.96	-1.60
<b>J2248-0101</b>	0.477233	7.1	368	159	1.72	1.16	1.5	0.13	-0.55	-1.25
52347-0612	1.181463	7.2	297	123	1.05	0.46	2.3	0.39	-0.31	-1.03

Table 5.1: Results of Strength Parameter analysis. **Pulsars** which has blank spaces in the ratio **columns** show slightly more rms noise than the white noise rms (i.e  $\sigma_R/\sigma_W < 1$  either in the minimum data block or in the maximum data block or in both, hence these ratios are not calculated).

calculated using eqn.(5.21) ( $\sigma_W$ ) and rms of the residuals ( $\sigma_R$ ) respectively. 'Signal-to-noise' ratio of the timing noise defined as  $\sigma_R/\sigma_W$  is listed in column (8). Logarithm of the strength parameter ratios estimated using equations (5.13, 5.14 & 5.15) are given in the last three columns.

Out of the 16 pulsars that we have, we find that the ratio  $\sigma_R/\sigma_W < 1$  for two pulsars and for seven other pulsars it is quite close to unity implying that there is no detectable slow variation (red noise) present in the residuals. But pulsars PSR 50459-0210, 51648-3256, 51901-0907 and **J2248-0101** have significant value for the ratio  $\sigma_R/\sigma_W$  and their  $\log(F_{PN})$ 's are close to zero i.e.  $F_{PN}$  is close to unity. As discussed in the section 5.2, this value of  $F_{PN}$  implies that the noise seen in the phase residuals of these pulsars can be explained by random walk in phase. In the case of PSR 51852-2610 it is quite confusing considering the value of  $\log(F)$  for phase noise and frequency noise whether the residual variation seen is consistent with random walk in phase or frequency and also its  $\sigma_R/\sigma_W$  is only 1.2. Whereas for the pulsar 52347-0612, the value of  $\log(F)$  suggests that the variation seen in the residuals is more consistent with the random walk in frequency rather than the random walk in phase. It is quite surprising to see that these pulsars show some similarities to random variation in phase and frequency in spite of their old ages ( $\sim 10^6 - 10^7$  yr). There is a definite indication of presence of red noise, which may not have timing noise origin, but could be due to other reasons such as free precession, planetary companions etc. For example PSR 51823-0154 shows a periodicity of  $\sim 5$  months in the residuals suggesting one of the above possibilities such as free precession or a presence of planetary companion for the above periodicity but only further observations can confirm whether it is an artifact or a true periodicity.

Our results are quite consistent with the existing theory that the timing activity is predominantly seen in young pulsars. In our sample, all pulsars have characteristic ages more than a million years, and more than half of them don't show any timing noise. But a few interesting cases in which the presence of red noise is seen are worth following up. Long term observations may help us to pin-down the possible sources of observed variations in the phase residuals. One of the main problems that we have faced in our analysis is that the present data span is very limited, namely, to only one year (even though we have a baseline of one and a half years, the continuous sampling is only over one year).

## Summary of this chapter

- **Strength Parameter Analysis** was carried out on the timing residuals for 16 pulsars to look for possible signature of Timing Noise.
- The analysis results suggest that four out of the 16 pulsars show consistency with phase noise (random walk in phase), one pulsar shows consistency with frequency noise (random walk in frequency). Another pulsar shows a periodicity of  $\sim 5$  months in the phase residuals. We find these 6 cases interesting considering that these pulsars are reasonably old. Further observations would help us to confirm the origin of these

**noise variations.**

- **The residuals in the rest of the pulsars is consistent with the 'white' measurement noise. This absence of the Timing Noise in large fraction of the cases (10 out of 16) is quite consistent with the existing understanding that the timing activity is significant more in young pulsars,**

## Chapter 6

# Large scale structure of the Magnetic Field in our Galaxy

### 6.1 Introduction

It has long been appreciated that celestial bodies are endowed with magnetic fields. Ancient mariners used the magnetic field of the Earth to navigate around the globe. At the turn of this century, the Zeeman effect detected in the spectrum of sun-spots implied the **existence of** solar magnetic fields. Recent advances in observational techniques have revealed the widespread existence of magnetic fields in the universe, and yield much firmer estimates of magnetic fields in interstellar and intergalactic space.

Optical polarisation observations have been carried out for many years towards galactic and extragalactic nebulae. At first the interpretation of this phenomenon was in terms of Rayleigh scattering of light by dust grains. Further optical polarisation observations in the galaxy led to a new alternative interpretation, namely that the polarisation is caused by dust grains which are aligned in the interstellar magnetic field. Intense nonthermal radio continuum emission produced by the relativistic electrons gyrating in the magnetic field emitting synchrotron radiation becomes an excellent probe of the magnetic fields in the galactic objects, galaxies and radio galaxies. Also, the Zeeman effect observed in HI clouds, and more recently in OH,  $\text{H}_2\text{O}$  maser observations have given a handle on magnetic fields in dense molecular clouds in the galaxy.

The study of the Faraday rotation in the direction of extragalactic sources and pulsars provides another way to probe the large scale magnetic field of the Galaxy. With this method, we get information about the field component parallel to the line of sight ( $B_{\parallel}$ ). Pulsars are excellent **probes** since they do not have intrinsic **Faraday** rotation and they offer the most direct method of determining  $B_{\parallel}$ . Electron density weighted magnetic field along a sight-line can be directly computed from the rotation measure (RM) and dispersion **measure** (DM) of pulsars.

## 6.2 Origin of the Magnetic fields

Two alternative models for the origin of magnetic fields **have** been proposed: (i) *primordial model* where the observed fields result from the compression of a relic field, and (ii) the *dynamo scenario* where the field is generated through the amplification of a seed field due to differential galactic rotation.

The primordial field model was developed in some detail by **Piddington(1964, 1978, 1981)**. In this scenario, the intergalactic ordered field was believed to be captured by a protogalaxy and then contracted and twisted by the differential rotation to generate a Bisymmetric Spiral (BSS) field. The BSS magnetic field structure seen in most of the spiral galaxies strongly suggests the existence of primordial intergalactic field. Evidence for an intergalactic magnetic field of the order of **1 nG** has also been suggested (Fujimoto et al 1971, Sofue et al. 1979, Weller et al. 1984). One of the drawbacks of this scenario as pointed out by **Parker(1979)** is that in the presence of turbulence the primordial field would be dissipated in **10<sup>9</sup>** years, which is much smaller than the age of the galaxy itself.

All the other recent theoretical investigations have been directed **towards** the interpretation of the magnetic fields in galaxies in the context of the turbulent hydromagnetic dynamo theory. **Parker(1971)** has suggested a concept of  $\alpha - \omega$  dynamo, where a mean **toroidal** field is generated from an original poloidal field by the non-uniform (differential) rotation  $\omega$ , and the **poloidal** component is produced from the toroidal field by the effects of cyclonic convection (the  $\alpha$  effect). Since observations of the magnetic field in the external galaxies suggest a dominance of BSS structure, numerous theoretical **investigations** were carried out to explain this observational fact. The solution of the **dynamo** equation (**Ruzmaikin et al. 1985, Sawa & Fujimoto 1986, Strachenko & Shukurov 1989**) showed that the co-existence of the Bisymmetric Spiral Structure and Axisymmetric Spiral Structure modes was possible in the context of the dynamo theory. The growth rates of different modes and the stability of the nonlinear dynamo have been discussed by **Brandenburg et al.(1989)**.

Both the primordial field concept and the galactic dynamo theory require some **seed** magnetic field. In the dynamo picture the seed magnetic field can be amplified by a factor of **10<sup>3</sup>** or more. In the non-linear dynamo the amplification factor could be even greater. Various possibilities for field generation were considered to occur in stars, galaxies and **supra-galaxy** phenomena, such as galaxy collisions, galaxy cluster-scale **infall** or 'Compton drag' or intergalactic plasma (for a detailed review, see **Kronberg 1994**). For example, since the electrons and the ions have the same charge but different masses, **differential compton drag** can potentially induce large scale currents in the interaction between the intergalactic plasma and the photon **flux** of the cosmic background radiation, which in turn will produce magnetic fields. Alternatively, extragalactic metal lines seen in QSO absorption lines which traces magnetized galactic winds allows one to argue that the **seed** fields with which most galaxies formed came from stars, since the stars are the origin of these **metal lines** and the observed galactic **magnetic** fields could have been the expelled stellar **fields** during **supernova** explosions.

The general trend of much of the observational evidence and the theories suggests that (i) magnetic fields were built up over times much shorter than galaxy lifetime and that (ii) spiral and **starburst** galaxies, as well as radio **jet/lobe** systems of radio galaxies are able to generate fields  $\sim$  microgauss in timescales  $\ll 10^8$  yr.

### 6.3 Methods of measuring Magnetic fields

The basic information about the presence and structure of magnetic fields is obtained from optical and radio observations. Optical polarisation observations show the presence of magnetic fields that align dust grains. These grains are apparently elongated and hence scatter light preferentially in one plane. Polarised radio emission originates due to the synchrotron process. While the plane of the polarisation is determined by the direction of the magnetic field, the intensity of the radio emission depends on the magnetic field strength. The latter fact with an assumption of **equipartition** of energy, allows us to estimate the field strength. In addition to this, the polarised wave suffers **Faraday** rotation in the interstellar plasma. By assuming an electron density distribution and the path length, one can estimate the strength of the line of sight component of the field from observed Faraday rotation measures.

#### 6.3.1 Zeeman effect

The Zeeman effect can be used in the optical and radio domain to directly measure the magnetic field strength. This effect is due to the fact that atomic or molecular electrons interact with a magnetic field leading to the splitting of a spectral line. In the simplest case the line is split into a triplet. The unshifted component corresponds to the transition that leaves the projection of the atomic angular momentum unchanged. This component is linearly polarised while the shifted components are circularly (left and right handed) polarised. Numerically the difference in the two shifted components in HI clouds is 2.8 Hz per  $\mu\text{G}$  (**Bolton & Wild 1957**). Similar detectability is achieved with the OH line where the frequency shift is 3.8 Hz per  $\mu\text{G}$ . The Zeeman effect in the **H<sub>2</sub>O** line **gives** a shift of only 1 Hz per **mG** and hence observations allow detection of only the stronger magnetic fields in regions of maser emission. In the optical range, such measurements are difficult **as** the Zeeman shift is small compared to the Doppler broadening of the lines.

#### 6.3.2 Optical Polarisation

The first evidence for interstellar magnetic fields came from measurements of optical **po**larisation of starlight (Hall 1949, Hiltner 1949). The **basic** mechanism (the so-called **Davis-Greenstein** effect) that is responsible for **the optical** polarisation is the scattering of light by elongated dust grains aligned by the magnetic fields (Davis & Greenstein 1951). This enables us to measure the linear polarisation of stars or of globular clusters in the nearest galaxies. **Optical polarisation measurements**, though indicate the orientation of the field,

do not yield estimates of the field strength. **The** field alignment is expected to be such that the polarised **E** vector is parallel to the field orientation.

### 6.3.3 Radio Polarisation

#### Radio Synchrotron emission

The synchrotron process (magnetic bremsstrahlung) is responsible for most of the low radio frequency radiation which is highly linearly polarised (**e.g.** **Ginzburg & Syrovatskii** 1969, **Pacholczyk** 1970). The synchrotron emission is generally elliptically polarised. The electric (**E**) vector of the linear component (which can be up to  $P_{\max} = (\gamma+1)/(\gamma+7/3) \approx 70 - 75\%$ , with  $\gamma$  the power spectral index of emitting electrons) is perpendicular to the orientation of the magnetic field. In some parts of the Galaxy, in nearby galaxies and in radio galaxies, linear polarisation of **upto** 70% has been detected indicating a high degree of ordering of the field. If the linear polarisation is mapped at several frequencies we can conclude about the orientation of  $\mathbf{B}_{\perp}$ , the component perpendicular to the line of sight, in the emitting region. To obtain the strength of the magnetic field equipartition between the energy density of cosmic rays and the magnetic field is assumed.

#### Faraday Rotation

Linearly polarised waves are subject to Faraday rotation when they pass through a magnetoionic plasma. The rotation angle is proportional to the magnetic field, the electron density, the distance of the source **from** the observer, and inversely proportional to the square of the wave frequency. It is customary to express the rotation angle ( $\phi$ ) in terms of the square of the wavelength as

$$\phi = RM\lambda^2 + \phi_0 \quad (\text{rad}) \quad (6.1)$$

The factor **RM** is termed "the rotation measure"<sup>n</sup>. In astrophysical units with the path length ( $l$ ) measured in parsecs, the electron density  $n_e$  in  $\text{cm}^{-3}$ , and the longitudinal field strength  $B_{\parallel}$  in  $\mu\text{Gauss}$ , it can be written as

$$RM = 0.81 \int_0^l n_e B_{\parallel} dl \quad (\text{rad m}^{-2}) \quad (6.2)$$

where the coefficient 0.81 has replaced the constants  $(e^3/2\pi m^2 c^4)$ . The **RM** is considered to be positive when the magnetic field is pointing towards the observer and it is negative when it is pointing away **from** the observer. By measuring the angle between the polarisation plane and a fixed reference direction at several (**atleast** two) suitably separated wavelengths one can determine the rotation measure, and then by extrapolating to  $\lambda = 0$  one can find **the** intrinsic position angle  $\phi_0$  of the polarisation of the source. For extragalactic radio sources **and pulsars**, **most** of these measurements have been made in the wavelength range of 0.9 cm to 74 cm. At longer wavelengths  $\phi$  may rotate through **many** radians within the

observing band resulting in depolarisation, while at smaller wavelengths (e.g. the optical range) the Faraday rotation is negligible. For Galactic and extragalactic radio sources bandwidths ranging from 10 **kHz** to a few **MHz** have been used. Also, the determination of RM is made difficult by the combination of **180°** ambiguities and measurement errors in the polarisation angle  $\phi$ . Under these circumstances the RM and  $\phi_0$  would have a non-unique answer. One of the ways to evade this **difficulty** is to take measurements at sufficiently closely spaced wavelengths. The other difficulty is due to the fact that Faraday rotation also takes place within the source itself where the radiation is generated.

Once the Rotation Measure is known, given the distance to the source and the electron density of the medium, the field projection onto the line of sight can be found. In the case of pulsars, the electron density weighted magnetic field along the line of sight **can** be computed from its rotation measure and dispersion measure (DM) as follows:

$$B_{\parallel} = 1.232 \frac{RM}{DM} \quad \mu\text{G} \quad (6.3)$$

The measurement of DM is directly possible through pulsar timing observations at suitably spaced frequencies.

## 6.4 Magnetic fields of external galaxies

Optical polarisation was first detected in M31 by **Ohman(1942)**. Further observations by **Muliarchik(1957)** and **Hiltner(1958)** suggested that the magnetic field orientation was along the spiral arms of M31. This optical polarisation is both due to the scattering of light, as well as due to the Davis-Greenstein effect.

Galaxies are mapped at radio frequencies by observing the synchrotron emission, which is emitted with E vector perpendicular to the orientation of the magnetic field. But this undergoes Faraday rotation due to the galaxy itself, the intergalactic medium and in our Galaxy. To correct the Faraday rotation effect one needs to have observations at several frequencies. The first published result on an external galaxy was by Mathewson et al.(1972) for **M51**.

The predominant configuration of the large scale field seen in most of the galaxies is bisymmetrical spiral structure. A few of them show axisymmetric spiral or circular ring field. The analysis of the magnetic fields, which was originally developed by **Tosa** and **Fujimoto (1978)**, involves the study of the rotation measure as a function of azimuthal angle  $\theta$  as illustrated in fig (6.1). Further details of such studies can be found in **Sofue et al.(1985)** and **Krause et al.(1989a,b)**

When the field has a Circular ring configuration or **axisymmetric** spiral structure (fig 6.1), then the line of sight component changes sinusoidally as a function of  $\theta$  along a circle concentric to the centre. Thus the rotation **measure(RM)** will **vary** as

$$RM = RM_0 \cos \theta \sin i \quad (6.4)$$

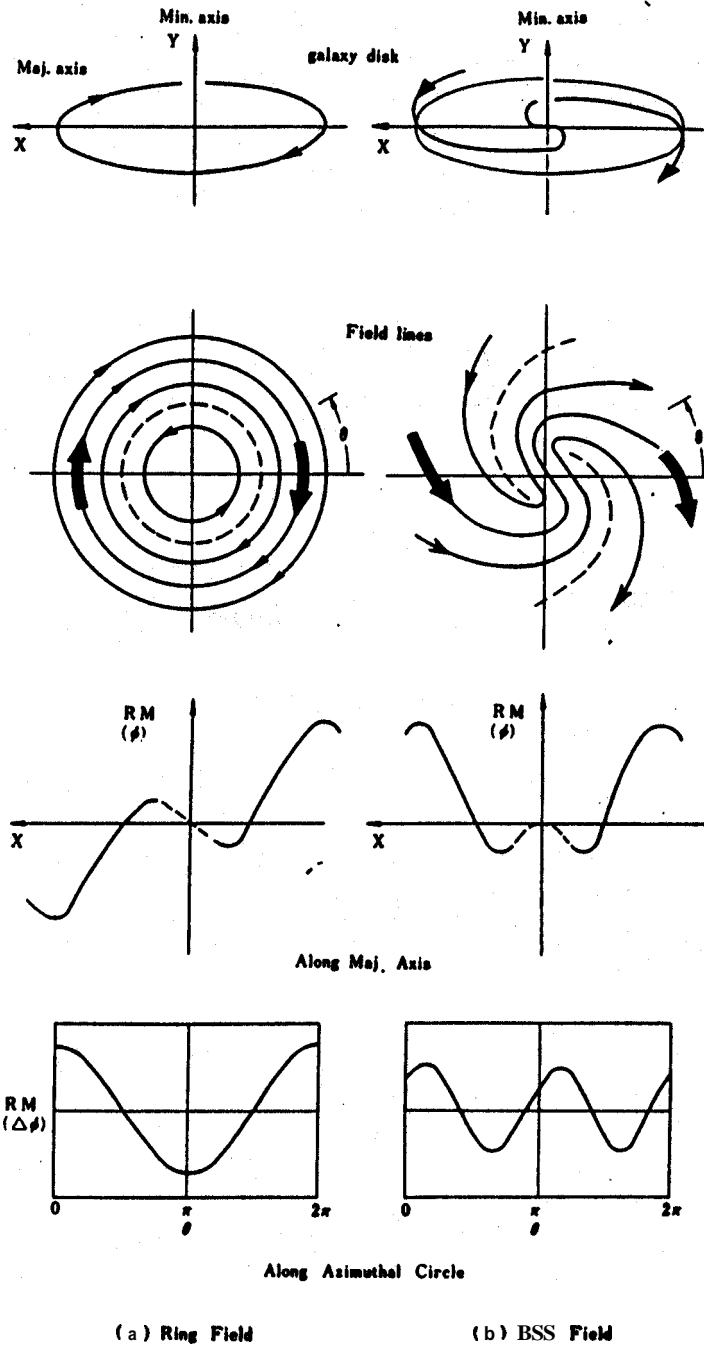


Figure 6.1: The ring and bisymmetric (BSS) magnetic field configurations in disk galaxies. The characteristic variations of  $RM$ ,  $\phi$ , or  $\Delta\phi$  are illustrated against the distance along the major axis and against the azimuthal angle  $\theta$  along a circle.

where  $i$  is the inclination of the galaxy. The characteristic rotation measure  $RM_o$  is defined by

$$RM_o = 0.81 \int_0^{\infty} n_e B_o(z) dz \quad (\text{rad m}^{-2}) \quad (6.5)$$

where  $B_o(z)$  is the field strength of the ordered parallel component along the circle as a function of the distance 'z' from the galactic plane.

If the field is a bisymmetric spiral, then the rotation measure varies with  $\theta$  in the following way (Tosa & Fujimota 1978, Sofue et al. 1980)

$$RM = \frac{1}{2} RM_o \tan(i) [\cos(2\theta - p - m) + \cos(p - m)] \quad (6.6)$$

where  $p$  is the pitch angle of the spiral field and  $m$  is the position angle at the maximum field strength on the circle. The essential difference between the above two equations is that the variation of the RM with the azimuthal angle  $\theta$  is a single sinusoidal for a ring field, whereas for a BSS field it is a **double-sinusoidal** (fig 6.1).

The observational facts with regard to the large scale magnetic field in the disks of spiral galaxies so far known from the **Faraday** rotation analysis may be **summarised** as follows: *the predominant configuration of the large scale field in a spiral galaxy is bisymmetric spiral (BSS) structure, with the field lines possibly open to the intergalactic space.* For example, M33 shows a clear BSS characteristic (Buczilowski 1985), with well ordered field in the northern half of the galaxy, whereas the field alignment and polarisation is low in the radio-bright region in the southern half of the galaxy. The latter result may be due to strong interstellar turbulence enhanced by star formation in the southern galaxy. Another class of galaxies show circular field structure like M31 which shows radio **emission** confined to a circular ring-like structure at a **galactocentric** distance **R=10** kpc. Another example of this class is a late type Scd spiral IC 342. In one of our nearby galaxy **NGC6496** Beck & Hoernes (1996) found that there are two well **defined** magnetic spiral arms lying between the optical arms, which is surprising because dynamo action is thought to be related to star formation activity, which is concentrated within or at the leading **edges** of the optical spiral arms. Field enhancement inbetween the **arms** can be understood in the sense that in the optical arm, the field tangling and the **Faraday** depolarisation would be higher than in the interarm. Edge-on galaxies, for example NGC 4631, show vertical field especially close to the nuclear area. Away from the **nuclues** the fields tend to change their orientation and follow the disk.

## 6.5 Magnetic field in our Galaxy

Starlight polarisation studies showed that the local field in our Galaxy has a high degree of uniformity (Mathewson & Ford 1970). At low galactic latitudes ( $b$ ), field is almost parallel to the galactic plane and at high  $b$ 's, the field is perturbed by the North Polar Spur. A recent investigation (Andreasyan & Makarov 1989) on the galactic magnetic field from an optical polarisation **dataset** on more than 7500 stars shows that the magnetic fields in the

galactic plane are **concentrated in the** spiral arms and directed along the axis of the arms. Zeeman splitting measurements shows that the **magnetic** fields in the molecular gas are closely related to the galactic **magnetic** field. More recent observations by Yusef-Zadeh & Morris (1987) and Haynes et al. (1992) show **polarised structures** perpendicular to the Galactic plane near the Galactic centre.

### 6.5.1 Rotation Measures of Extragalactic sources

A **common** way to estimate the large scale magnetic field in our galaxy is to use rotation **measures** in the direction of extragalactic radio sources like quasars and radio galaxies. As **derived** from radio RM observations of QSO and galaxies (first reported by Morris & Berge 1964), the local magnetic field near the Sun points towards the galactic longitude  $l \approx 90^\circ \pm 15^\circ$ , with a strength for the regular component of  $\approx 2\mu\text{G}$ , and with a somewhat bigger random component. Simard-Normandin & Kronberg (hereafter SK 1980) **analysed** 552 **RMs** and found several specific local galactic features in the **RM** map of the sky, such as 'Region A' and the North Galactic Spur (Loop I). They showed that a bisymmetric 4-arm spiral field model, with pitch angle of  $-14^\circ$ , and having field reversals could reproduce the principal observed features in the **RM** map. Sofue & Fujimoto (1983) showed that a large scale magnetic field in our galaxy is oriented along the spiral **arms** and the field lines change their direction from one arm to the next across the neutral line in the **interarm** region. The loci of maximum field strength trace the spiral arms defined by HII regions. **Vallee** (1991) argued that the global magnetic field of our Galaxy is axisymmetric in configuration, but is not a concentric ring. **Vallee** (1995) in a statistical study to estimate the pitch angle, number of arms, and global shape using observations since 1980, obtains a **mean** pitch angle value  $p = -12^\circ \pm 1^\circ$  and a median number for spiral arms as 4.

### 6.5.2 Rotation Measures of Pulsars

Pulsars can be very **useful** probes to determine the **magnetic** field of our galaxy for several reasons. Firstly, their approximate distances can be estimated from their **DMs**. Secondly, they do not have any intrinsic **Faraday** Rotation, as the polarisation characteristics pattern of a pulsar at different **frequencies** are very similar to one another. Thirdly, the mean **line-of-sight** component of the magnetic field (though weighted by the electron density) **along** the path to a pulsar can be obtained directly from the ratio of its rotation measure to its dispersion measure.

Manchester (1974) using **RMs** of 28 pulsars found that the local field (close to the Sun) is directed towards  $l = 94^\circ \pm 11^\circ$  with a strength of about  $2.2 \pm 0.4 \mu\text{G}$ . **Thomson** & Nelson (1980) used 48 pulsars within 3 kpc from the Sun and a five parameter model to derive the local magnetic field and **found** a field reversal at distance  $170 \pm 90$  pc from the Sun. They found that the field is directed along  $l = 74^\circ \pm 10^\circ$  in the solar vicinity, with a strength  $B = 3.5 \pm 0.3\mu\text{G}$  and a low scale-height of 75 pc. **Lyne** & Smith (1989) analyzed the **RMs** and **DMs** of 185 pulsars and got results very **similar** to those

by Manchester (1974) and Simard-Normandin and Kronberg (1980, hereafter SK). Chi & Wolfendale (1990) confirmed the field reversal and the field direction obtained by Thomas & Nelson (1980). **Andreasyan & Makarov** (1989) found a 'halo' component besides the flat component, from the **RM**s of 185 pulsars.

Rand & **Kulkarni** (1989) used rotation measures for about 118 pulsars within 3 kpc to reveal the local galactic field towards  $l = 94^\circ \pm 4^\circ$  with a strength  $B = 1.6 \pm 0.2 \mu\text{G}$ . **Relaxing** the 3 kpc limit, they found that a concentric ring model was a better description than a bisymmetric spiral model. They estimated the field strength (at the position of the sun)  $B_\odot = 1.3 \pm 0.2 \mu\text{G}$ , and reversals at 2450 pc outside the solar circle and at 650 and 3250 pc inside it. They **also** used the variance and covariance of the best-fit residuals to model the random magnetic field, for which they obtained a field strength of  $\approx 5 \mu\text{G}$  and a cell length of  $L \approx 55$  pc. Through a careful selection of pulsars for their analysis, **Han & Qiao** (1994) found that the Galaxy has a global field of **BiSymmetric** spiral (BSS) configuration rather than a concentric ring or an Axisymmetric Spiral (ASS) configuration. For the BSS structure, they obtain pitch angle of  $-8.2^\circ \pm 0.5'$  and an field amplitude of  $1.8 \pm 0.3 \mu\text{G}$ . They also found that the field is strong in the **interarm** regions and it reverses in the arm regions. **Han et al. (1996)** have identified a striking antisymmetric pattern about the Galactic plane and the meridian through the Galactic Centre from the distribution of **RM**s of extragalactic sources and the **RM**s of pulsars with  $|b| > 8^\circ$ . This indicates that a dynamo mode of odd symmetry, possibly of **A0** type, makes a substantial contribution to the magnetic fields in the thick disk and halo of our Galaxy, at least inside the Solar circle.

## 6.6 Modelling the Magnetic field using Rotation Measures of Pulsars

We have tried to explore the possibility of refining the description for the magnetic field distribution in our galaxy using the rotation measures of pulsars. As already mentioned, such attempts have been made by many groups so far and these have resulted in a variety of models. However, it should be pointed that **these models** have assumed a constant value for the electron density throughout the galaxy. In our attempts to model the galactic magnetic field, we have used a recent comprehensive model of the electron density distribution (**Taylor & Cordes** 1993) which has explicitly allowed for the electron density variations due to the spiral structure in our galaxy. Also, we explored the possibility that the magnetic field strength and the electron density may have correlated variations; for example, field being relatively high in the spiral arm regions **compared** to the inter-arm regions or vice versa. Our analysis **software** code used for this **was** first tried with earlier models available in the literature and **was** checked to reproduce consistent results. We have examined four models: one model for the local field and three models for large scale magnetic field distribution by incorporating the Taylor-Cordes electron density model. The description of the various models is given below.

### 6.6.1 Description of the Models

- Longitudinal Model:

So far, the observational evidence shows that the local galactic magnetic field is longitudinal in direction **and is** pointing towards  $l \sim 90^\circ$  with an average strength of  $\sim 2 - 3 \mu\text{G}$ . Also, many groups have noticed a field reversal towards the galactic centre within a distance of 0.5–1 kpc from Sun.

It is required that any best-fit model obtained for large scale field should **also** be consistent with the strength and the direction of the field in the solar vicinity. With this view and also to enable comparison of our results with the earlier results, we have attempted modelling the local field using four parameters: (i) the magnetic field strength  $B_0$ , (ii) direction  $l_0$ , (iii) the distance,  $d_r$ , of the field reversal from Sun, and (iv) the width of the transition region,  $\Delta d_r$ , over which the field reversal occurs. Here we have modelled the field to reverse smoothly (.with a linear change) rather than abruptly **as** considered by earlier groups.

- Concentric ring Model:

In this model, the field has only an azimuthal component and no radial component. The model can be described by

$$B_r = 0 \quad (6.7)$$

$$B_\theta = B_0 \sin \left[ \frac{\pi}{W} \{r - (R_0 - d_r)\} \right] \quad (6.8)$$

where  $W$  is the spacing between the reversals,  $d_r$  is the distance of the first reversal in direction of  $l \sim 90^\circ$  and  $B_0$  is the peak amplitude of the magnetic field. In this model, the field varies sinusoidally as a function of galactocentric radius. Such a field geometry can be produced by galactic dynamo models of the field in which a symmetric azimuthal mode is dominant. Reversals of the field **as** a function of galactocentric radius are also predicted by this theory. Theories involving a primordial origin of the field also claim to be able to produce ring fields, but only in the inner regions of galaxies (Sofue, **Fujimoto** and Wielebinski 1986). Rand and **Kulkarni** (1989, hereafter RK) have suggested that a circular **geometry** with field reversals gives more appropriate fit to the pulsar RM data.

- Bisymmetric Spiral Model:

A **4-arm** logarithmic spiral model of the global magnetic field **was** first used by SK (1980) to reproduce the features in the RM distribution of extragalactic radio sources. Sofue **and Fujimoto** (1983) used a two-arm **BSS** model with a pitch angle of a fixed value of  $-5^\circ$  to reveal the main features of the RM distribution. RK (1989) use **the formulation** of Sofue and **Fujimoto** (1983) to fit the **RMs** of pulsars, but they get a positive pitch angle. But, Han & **Qiao** (1994) **found** some inconsistencies in the definition of BSS model of Sofue **and Fujimoto** and have therefore rederived the

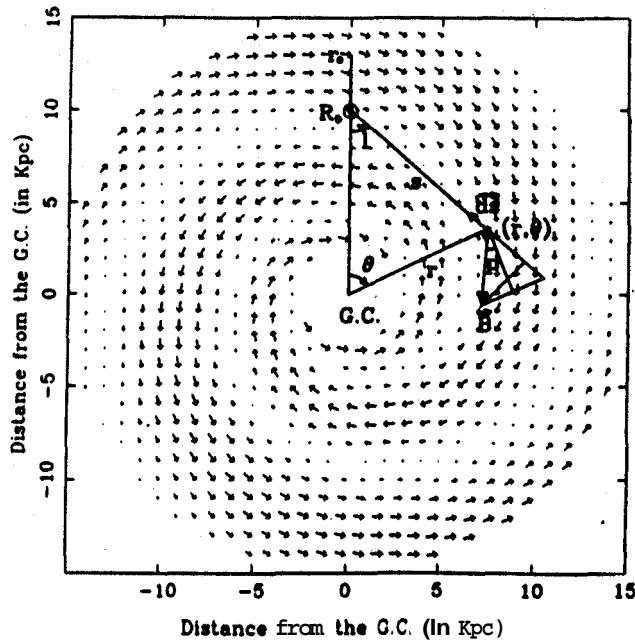


Figure 6.2: A bisymmetric logarithmic open-spiral configuration in the galactic plane. The field directions are indicated by the arrows. The size of arrows is proportional to the field strengths. The geometrical meanings of  $r_0, R_0, l, \theta, r, s, p$  &  $ds$  are indicated in the figure.

equations for the BSS model. We also have examined this aspect independently and find the equations by Han & Qiao to be correct. The structure of **this** type of field is shown in fig(6.2) and can be expressed in the following form.

$$B_r = B_0(r) \cos\left(\theta - \beta \ln \frac{r}{r_0}\right) \sin p \quad (6.9)$$

$$B_\theta = B_0(r) \cos\left(\theta - \beta \ln \frac{r}{r_0}\right) \cos p \quad (6.10)$$

where

$$r = (s^2 + R_0^2 - 2sR_0 \cos l)^{1/2} \quad (6.11)$$

$s$  is the distance of the point  $(r, \theta)$  from the Sun,  $R_0$  is the distance of the Sun from galactic center,  $\beta = \frac{1}{\tan p}$ ,  $p$  being the pitch angle of the spiral,  $l$  is the longitude of the sight-line,  $B_0(r)$  is the magnitude of the field as a function of **r-galactocentric** distance. At the point  $(r = r_0, \theta = 0^\circ)$ , the field strength reaches the first maximum  $B_0(r_0)$  in the direction  $l = 180^\circ$  outside the solar circle.

No theory of the magnetic fields of galaxies has any explicit suggestion for the form of the function  $B_0(r)$ . So far, the detailed measurements of a bisymmetric field in M51 (Horellou et al. 1992) show that the field strength decreases slowly from

the center to the outskirts of M51. RK (1989) and Han & Qiao (1994), however, have assumed  $B_o(r)=\text{constant}$  in their work, while Sofue and Fujimoto (1983) favour  $B_o(r) = (3R_o/r) \mu\text{G}$ . We have assumed the  $B_o(r)$  as a constant  $B_o$ , but we have considered this planar field  $B_o$  to decay exponentially as the **z-distance** from the galactic plane increases. In addition to this planar field, we have also included a z-component of the magnetic field ( $B_z$ ) which is modelled to decrease exponentially with increasing galactocentric distance ( $r$ ).

- **Magnetic field along (or in between) the spiral arms**

In this model, we have considered two cases:

(i) The magnetic field parallel to the galactic plane is assumed to be maximum along the spiral arms and the field undergoes a reversal smoothly in between the spiral arms. So the field at centres of the adjacent spiral **arms** will have maximum strength but opposite sign. To identify the position of the spiral arms along the line of sight to the pulsar we have used the Taylor-Cordes electron **density** model. In this model we have also considered the possibility of the magnetic field being dependent on the local value of the electron density as follows:

$$|B(x, y, z)| = B_o(1 + k\sqrt{n_e(x, y, z)}) \quad (6.12)$$

where  $k$  is the proportionality constant and the dependence of electron density **ap-**pears **as** a modulation around the constant magnetic field  $B_o$ . The dependence on the electron density is modelled to be consistent with an equipartition between the energy densities of the magnetic field **and** the thermal **electrons**. This model has only two free parameters namely  $B_o$  and  $k$ .

(ii) The magnetic field in this case is assumed to be strong in the **interarm** regions with **smooth** reversal at the centre of the spiral arms. Here **we** haven't assumed any dependence on electron density for magnetic field and have tried to fit only for the peak field strength  $B_o$ .

In both the cases, a vertical component of the field (the z-component) was also considered to assess possible improvements in the fits.

## 6.6.2 The Modelling Procedure

✎ Considering each of the models described above, the rotation measures calculated for all the selected pulsars as follows:

$$RM_{\text{cal}} = -0.81 \sum_{i=1}^{n_{\text{step}}} n_e(x, y, z) B(x, y, z) d_{\text{step}} \quad (6.13)$$

where  $x, y$  are the galactocentric **coordinates** in the galactic plane. We have **taken**  $d_{\text{step}}$  to be 10 pc and  $n_{\text{step}}$  is the number of such steps along the sight-line to the pulsar. Note that **the** electron density  $n_e$  **along** the path **and** the **distance** to the pulsar are obtained

from the Taylor & Cordes (1993) electron density model.  $B(x, y, z)$  is the field strength at  $(x, y, z)$  obtained from the chosen model. For a particular model, a measure of the difference between observed and calculated RM is obtained by defining a chi-square as follows:

$$\chi^2 = \left( \frac{1}{\sum w_i} \right) \sum_{i=1}^{n'_{\text{par}}} \left[ \frac{RM_{\text{obs}} - RM_{\text{cal}}}{\sigma_{\text{RM}}} \right]^2 w_i \quad (6.14)$$

where  $\sigma_{\text{RM}}$  is the measurement error on the observed RM. For those pulsars whose  $\sigma_{\text{RM}}$  is less than 0.5, we have assumed it to be 0.5 because the uncertainties in calibration of the Faraday rotation due to the ionosphere are of this order. This also avoids the situation where a few (low  $\sigma_{\text{RM}}$ ) pulsars 'dominate' the  $\chi^2$  value. The term  $w_i$  is the weightage used for each pulsar. As seen in **fig(6.3)**, the observed distribution of pulsars projected in the galactic plane is not uniform. The concentration of pulsars seen in the vicinity of the Sun is due to selection effects in the detection of pulsars. If one gives equal weightage to all the pulsars in the calculation of  $\chi^2$ , the model for the large scale field will be constrained largely by the local objects and may represent the field which is more local rather than for the whole galaxy. Hence we have used  $w_i = (d/2)$  for pulsars whose distance from the Sun is less than 2 kpc and  $w_i=1$  otherwise. Also, note that the  $\chi^2$  contribution from all the pulsars in the sample ( $n_{\text{par}}$ ) is not included. The top ten percent contributors to  $\chi^2$  are rejected in the summation, i.e.  $n'_{\text{par}} = 0.9 * n_{\text{par}}$ . This would ensure that the resultant 'best-fit' solution is the one that is favoured by a reasonably large fraction of the sample used. Also, we calculate a quantity  $\chi_0^2$  using the above equation by forcing  $RM_{\text{cal}}$  to be zero for the same set of pulsars that are used to calculate  $\chi^2$ . This helps us to assess the significance of the best-fit parameters. In addition to this, for each model the percentage number of sign matches between observed RMs and the calculated RMs are noted. Finally the model which gives minimum  $\chi^2$  as well as maximum percentage of sign matches is considered as the most favoured model for the large scale structure of the magnetic field in our galaxy.

### 6.6.3 The selection of the sample of pulsars

Although more than 700 pulsars have been discovered so far, rotation measures are available for only about 250 pulsars. Most of these pulsars are located within 5 kpc distance (see **fig 6.3**). In fact, not all pulsar **RMs** can be used for modelling. It is important to identify the local features in the sky, such as nearby supernova remnants, ionised hydrogen **regions** which would give anomalous **RMs** over regions of large angular extent. Pulsars lying behind such regions should not be included in any modelling since their **RMs** may systematically bias the best-fit solution for the parameters.

One of such regions is the North Polar Spur (NPS). This region is nearby ( $D \sim 100\text{pc}$ ) and is roughly in the direction of  $l = 30^\circ$ ,  $0^\circ < b < 25^\circ$ . It is seen as a continuum feature which forms a part of **Loop-I** which is thought to be a nearby supernova remnant. The NPS and Loop-I have been studied by many workers (see a review by Salter, 1983). **Rickard** and **Crony11(1979)** suggest that there is an extended region ( $45^\circ < l < 75^\circ$ ,  $10^\circ < b < 65^\circ$ )

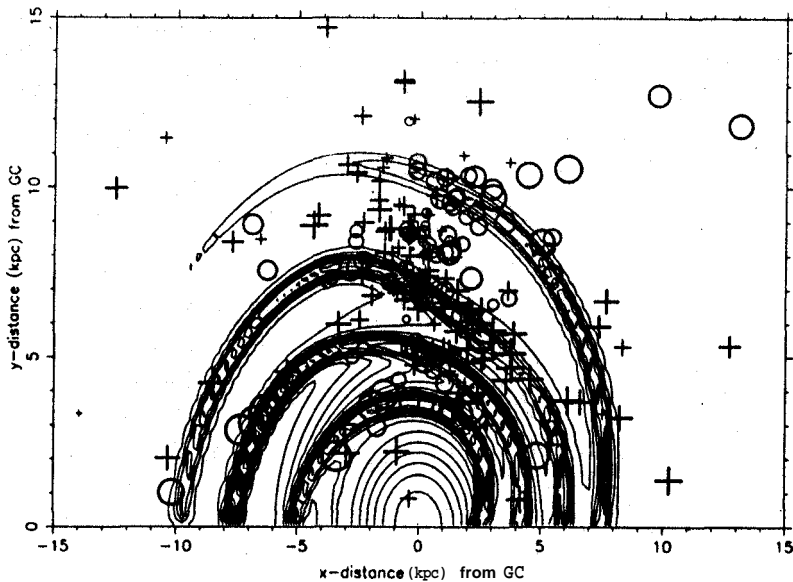


Figure 6.3: The distribution of pulsars in our Galaxy. The size of the marks '+' and 'o' indicate the magnitude and sign of the Rotation Measures. '+' represent a positive RM and 'o' represent a negative RM. This figure shows only one half of the galaxy towards Sun from Galactic Centre. The contours represent the spiral arms of our galaxy.

of enhanced turbulence which may be associated with the NPS. The pulsars whose sight-lines cross this NPS region are therefore removed from the analysis. Another such region, known as the Gum Nebula, is an ionised hydrogen region ( $l = 260^\circ, b = 0^\circ$ ). This region, about 400 pc away from the Sun, is located close to the Galactic plane and has an angular diameter of  $\sim 36^\circ$ . The effect of this nebula is clearly seen in the electron distribution (Lyne et al 1985), showing an enhanced electron density of about  $0.28 \text{ cm}^{-3}$ . Although the magnetic field in the shell is only about  $2 \mu\text{G}$ , the RM contributed by its shell might be as large as  $130 \text{ rad m}^{-2}$  (Vallee 1984). Hence we have excluded those pulsars whose sight-line crosses the Gum Nebula from our modelling.

Although there are two more special regions, 'Region A' and 'Monogem Ring', we did not remove from our sample all those pulsars whose sight-lines cross these regions as this would reduce the usable pulsar sample drastically. Instead, we have put an upper limit on the estimated  $B_{\parallel}$ , where  $B_{\parallel}$  is estimated as  $1.232 \times RM/DM$ , for pulsars to be included in the modelling. This avoids rejection of sample members unless the contaminations from these regions is significant. Considering the earlier estimates of the field strength which range from  $1.5$  to  $3.0 \mu\text{G}$ , we choose the  $B_{\text{limit}}$  to be  $3.0 \mu\text{G}$ . Further, as the structure of the magnetic field close to the galactic center is still not quite understood, we discard the pulsars whose galactocentric distance is less than  $4.0 \text{ kpc}$ . Also, the pulsars with  $z$ -distances (from the galactic plane) greater than  $1 \text{ kpc}$  are not included in the analysis, due to possible large uncertainties in their distances. After all this filtering totally 131

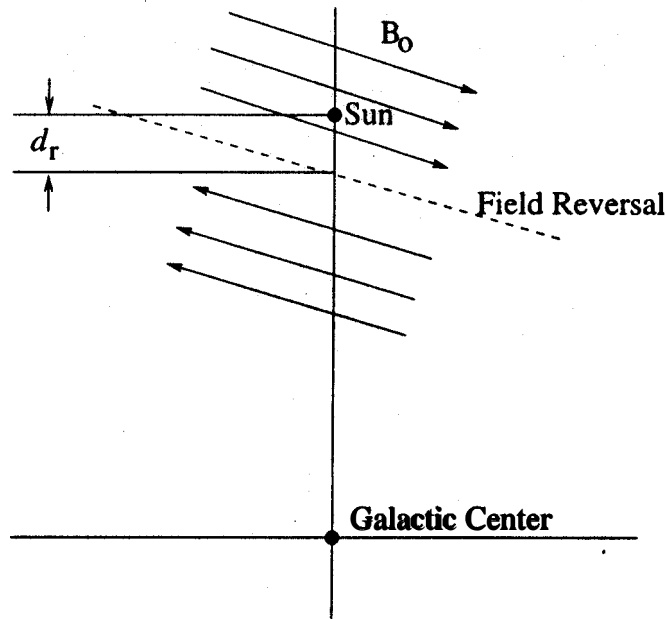


Figure 6.4: Schematic diagram of the longitudinal model.

pulsars were used for the modelling.

#### 6.6.4 Results and Discussion

- Longitudinal Model

To obtain the local field we have chosen 83 pulsars lying within a distance of 3 kpc from Sun. Our modelling shows that the local galactic magnetic field has a strength of  $1.8 \pm 0.1 \mu\text{G}$  pointing in the direction  $l = 70^\circ.7 \pm 2^\circ.6$ . The first field reversal occurs at a distance ( $d_r$ ) of  $1.1 \pm 0.05$  kpc towards the galactic centre direction. The transition distance over which the reversal occurs is found to be  $\lesssim 80$  pc, which would suggest a reasonably sharp reversal. A schematic diagram of this field is shown in fig (6.4). The minimum  $\chi^2$  obtained is  $\sim 88$  compared to the  $\chi^2_0$  of 437 and the number of sign matches is 64%. Figure (6.5) shows the comparison of the observed distribution of **RMs** with the predicted distributions of **RMs**.

- Circular ring model

Removing the 3 kpc limit on the pulsar distance, we have used 131 pulsars to derive the magnetic field using the rest of the models.

In the case of the circular ring model, the field is assumed to vary **sinusoidally** with the galactocentric radius. We have tried to fit four parameters in this model; namely (i) the field strength at **maximum**  $B_0$ , (ii)  $W$ : spacing between the reversals, (iii)  $d_r$ : the **distance** (from the Sun) at which **the** first reversal occurs, and (iv) the

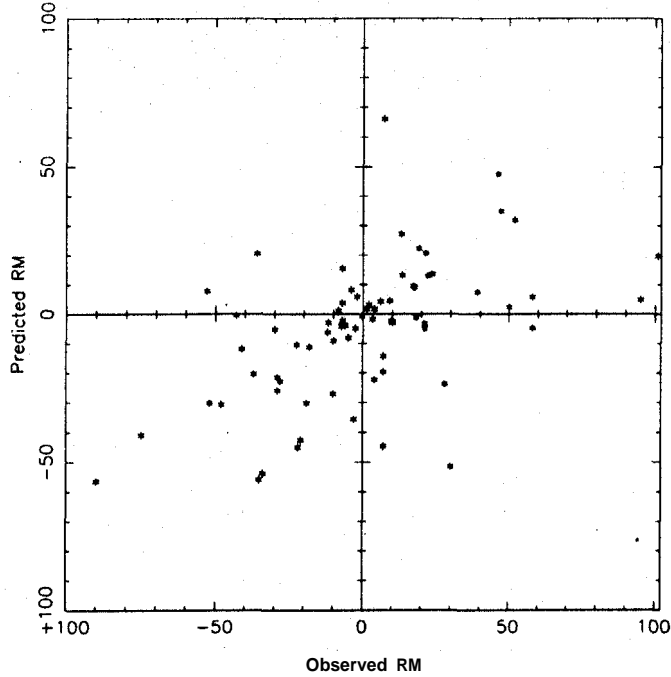


Figure 6.5: The correlation between the observed and the predicted **RM**s for the best-fit parameters for the local field can be seen from this figure.

characteristic height  $z_0$  from the plane at which the concentric azimuthal field drops to  $1/e$  of its value in the plane. The distance of the **Sun** from the galactic centre  $R_{\text{sun}}$  has been taken to be **8.5 kpc**. We obtained in a weighted fit

$$B_0 = 2.2 \pm 0.1 \mu\text{G}$$

$$W = 2.43 \pm 0.04 \text{ kpc}$$

$$d_r = 0.65 \pm 0.02 \text{ kpc}$$

$$z_0 = 3.89 \text{ kpc}$$

for the minimum  $\chi^2$  of **167** compared to a  $\chi^2_0$  of **552.3**. When we reduced  $z_0$  by **3 kpc** from the best-fit  $z_0$ , the  $\chi^2$  increased by **1**, but the  $\chi^2$  increase was very slow when  $z_0$  was increased from the best-fit value. The percentage **number** of sign matches is **64%**. When we include a vertical component of magnetic field in addition to the azimuthal component, the best-fit parameters are as follows:

$$B_0 = 1.9 \pm 0.1 \mu\text{G}$$

$$W = 2.9 \pm 0.2 \text{ kpc}$$

$$d_r = 0.68 \pm 0.03 \text{ kpc}$$

$$z_0 \simeq 20.4 \text{ kpc}$$

$$\text{and } B_z \exp\left(\frac{-R_{\text{sun}}}{R_s}\right) = 0.23 \mu\text{G}$$

for  $\chi^2$  of  $\sim 179$ . We found that  $\chi^2$  drops, though very slowly, as  $B_z$  increases  $R_z$  started decreasing simultaneously keeping the field near the Sun almost constant. The percentage number of sign matches increased from 64% to 69% when we considered the vertical component which may be considered as an indication of the presence of the vertical field.

- **Bisymmetric Spiral field**

The free parameters in this model are the strength of the magnetic field  $B_o$ , the pitch angle  $p$  of the spiral, the distance  $r_o$  at which the field attains its first maximum, the scale height  $z_o$  of this spiral field in the direction perpendicular to the galactic plane, the vertical field  $B_z$ , and the galactocentric distance  $R_z$  at which  $B_z$  drops by  $1/e$  of its value at the centre of the galaxy. We have performed a model fit using equations (1.9) and (6.10) for the selected sample of 131 pulsars. The best parameters found are

$$B_o = 2.29 \pm 0.12 \mu\text{G}$$

$$p = -6^\circ.75 \pm 0^\circ.13$$

$$r_o = 9.266 \pm 0.003 \text{ kpc}$$

$$z_o = 2.9(+7, -1.3) \text{ kpc}$$

$$\text{and } B_z \exp\left(\frac{-R_{\text{sun}}}{R_z}\right) = 0.21 \mu\text{G}$$

in the solar vicinity for minimum value of  $\chi^2 = 137$  while  $\chi_o^2 = 551.9$ . The percentage number of sign matches is 71%. To compare our results with those of Han & Qiao, we performed the fit for only azimuthal spiral field which yielded the following results of

$$B_o = 2.2 \pm 0.12 \mu\text{G}$$

$$p = -7^\circ.53 \pm 0^\circ.06$$

$$r_o = 9.41 \pm 0.02 \text{ kpc}$$

$$\text{and } z_o = 5.3 \text{ kpc}$$

( $\chi^2$  reducing slowly with high  $z_o$ ) for a minimum value of  $\chi^2 = 143.5$ , the percentage sign matches of 70%. For the same model with Han & Qiao's best-fit parameters  $B_o = 1.8 \pm 0.12 \mu\text{G}$ ,  $p = -8^\circ.3 \pm 0^\circ.06$  and  $r_o = 9.41 \pm 0.02 \text{ kpc}$ , the minimum  $\chi^2$  is  $\sim 225$  which is quite large compared to that corresponding to the best-fit parameters in our analysis.

- **Magnetic field along/inbetween the spiral arms**

The assumption of the field being maximum along the spiral arms has given a very poor fit for the observed rotation measures of pulsars. In this model, we attempted to see whether there is any correlation between the large scale magnetic field and the electron density distribution. The best-fit parameters of this model are  $B_o = 1.0 \pm 0.09 \mu\text{G}$  which is the background uniform field and the modulation constant  $k$

is  $3 \pm 1$  with  $\sqrt{n_e}$  ranging from 0.00854 to 0.2188  $\text{cm}^{-3}$ . However the corresponding  $\chi^2$  value of 416 ( $\chi_0^2 = 533$ ) is quite high compared to those for the other models and the percentage number of sign matches is also comparatively small, only 57%. In this model, we have not incorporated any explicit scale height for the field, instead the field variation in the **z-direction** would be that implied by the electron density variation itself.

In the other version of the model where the field inbetween the **spiral arms** (rather than at the arms) is strong, the best-fit model parameters are  $B_0 = 1.52 \pm 0.12 \mu\text{G}$  and  $z_0 = 28.3(-23)$  kpc for minimum value of  $\chi^2 = 228(\chi_0^2 = 425)$  with 60% sign matches in RM. If we include the vertical component for magnetic field  $\chi^2$  reduces to 197 from 228 and the percentage sign matches increases to 65%. The best-fit model parameters are

$$\begin{aligned} B_0 &= 1.89 \pm 0.12 \mu\text{G} \\ z_0 &= 19.5 \text{ kpc} \\ \text{and } B_z \exp\left(\frac{-R_{\text{sun}}}{r_{0z}}\right) &= 0.5 \mu\text{G}. \end{aligned}$$

Here we found  $\chi^2$  reducing slowly as  $z_0$  increases.

The best-fit results for all the models are briefly summarised in Table (6.1). The results of the model-fit for the last three **models** suggest that the Bisymmetric Spiral Field gives a better fit to the observed **RMs** of pulsars. Even though the percentage sign matches for **Circular** field is quite close to that for the BSS field, the value of  $\chi^2$  shows that BSS field model is preferred to that with the circular field. In almost all the models where vertical component for magnetic field is included in the fit, we found that  $\chi^2$  value reduces very slowly when  $B_z$  increases. But simultaneously the exponential scale height **also** decreases in such a way that  $B_z$  value remains more or less constant (0.2 –0.5  $\mu\text{G}$ ) in the solar vicinity. Also we found that the  $\chi^2$  **was** quite insensitive to  $z_0$ , the scale height of the planar field possibly because we have used pulsars whose **z-distances** are less than a kpc and hence the planar field is almost constant within this distance from the galactic plane.

**Circular** ring model (see fig 6.6) shows that there is one **reversal** outside the Solar circle at a distance of  $\sim 10.7$  **kpc** from Galactic centre and two reversals inside the solar circle at a distance of 7.8 kpc and 5 kpc **from** galactic centre. BSS field (fig 6.7) shows a field reversal at 11.3 kpc outside the solar circle and similar to circular ring model, there are two reversals one at 7.75 kpc **and** the other at 5.25 kpc. Both these field looks more or less **similar** with respect to the reversals, but the value of  $\chi^2$  suggests that BSS field model may be a better description for the magnetic field in our galaxy.

Also, we find that the peak magnetic field inbetween the spiral **arms** (see fig 6.8) is preferred compared to the peak field at the centres of the spiral **arms**; contrary to what **was claimed** by Sofue **and** Fujimoto (1983). Whereas our conclusion is consistent with that **by** Han & Qiao, who **suggest** that the field is strong in the interarms regions and reverses in the **arm** regions. If we **compare** the BSS field with the spiral structure (**fig6.7** and fig

Models for Planar Field	$\chi^2$	$\chi_0^2$	% SM	$B_0$ ( $\mu\text{G}$ )	Other Parameters	$B_z$ at Sun ( $\mu\text{G}$ )	
Longitudinal (a)	88	437	64	1.8	$\iota: 70^\circ.7; d_r: 1.08; \Delta d_r \lesssim 0.08$	-	
Circular Ring	(a)	167	552	64	2.2	$W: 2.4; d_r: 0.65$	-
	(b)	179	552	69	1.9	$W: 29; d_r: 0.68$	0.23
Bisymmetric Spiral	(a)	144	552	70	2.2	$\rho: -7^\circ.53; r_0: 9.41$	-
	(b)	137	552	71	2.3	$\rho: -6^\circ.75; r_0: 9.27$	0.21
Correlated with arms	(a)	416	533	57	2.4	$B = 1.0(1 + 3\sqrt{n_e})$	-
	(b)	254	283	57	0.06	$B = 0.002(1 + 60\sqrt{n_e})$	0.51
Anticorrelated with arms	(a)	228	425	60	1.5	-	-
	(b)	197	425	65	1.9	-	0.5

Table 6.1: A brief summary of the best-fit results for all the attempted models. First column gives the name corresponding to the model examined, column 2, 3 & 4 lists the  $\chi^2$ ,  $\chi_0^2$  and the percentage sign matches for the respective models. Column 5 gives the peak magnetic field strength of the planar field and column 6 lists the values for the other parameters in the respective models. Here  $d_r$ ,  $W$ ,  $r_0$  and  $Ad$ , are in kpc and  $n_e$  is in  $\text{cm}^{-3}$ . The last column lists the strength of z-component of the magnetic field in the Solar vicinity. (a) corresponds to the model having only planar field and (b) corresponds to the particular model with both planar and the z-component. For longitudinal field, only 83 pulsars within 3 kpc of Sun are used for modelling whereas for other models 131 pulsars distributed on one half of the galaxy are used.

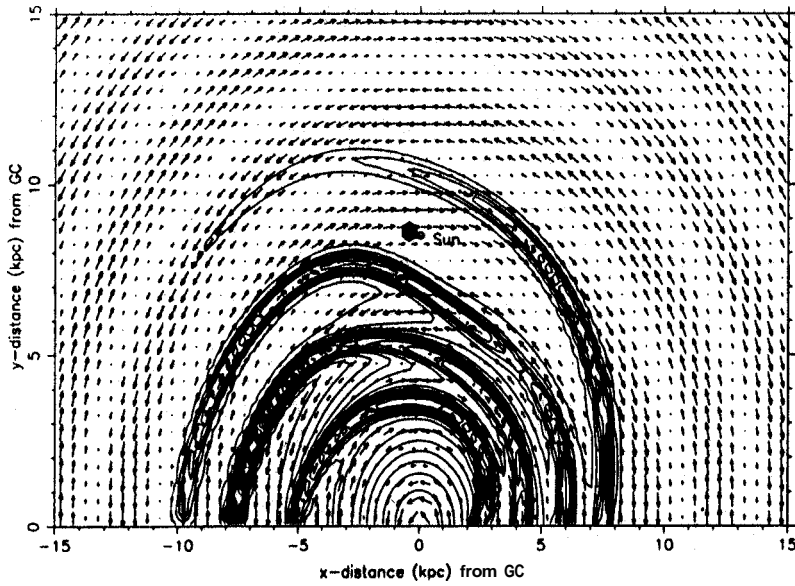


Figure 6.6: Magnetic field having a circular symmetry with the spacing between the reversals as 2.9 kpc and the first reversal from Sun at 0.68 kpc. The position of the Sun is marked by circled dot. The contours represent the spiral arm structure of the Galaxy and the arrows denotes the magnetic field and the length of the arrows represents the magnitude of the field at that point.

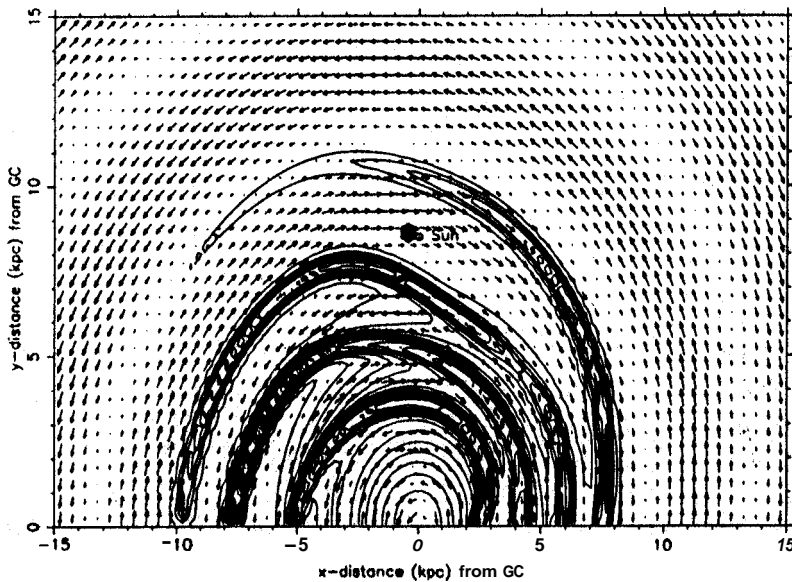


Figure 6.7: **Result** of the Bisymmetric field model-fit for the magnetic field for our Galaxy, obtained by modelling the RMs of 131 pulsars. The contours represent the spiral **arm** structure of the Galaxy and the arrows denote the direction of the magnetic field and the length of the arrow represents the magnitude of the field at that point.

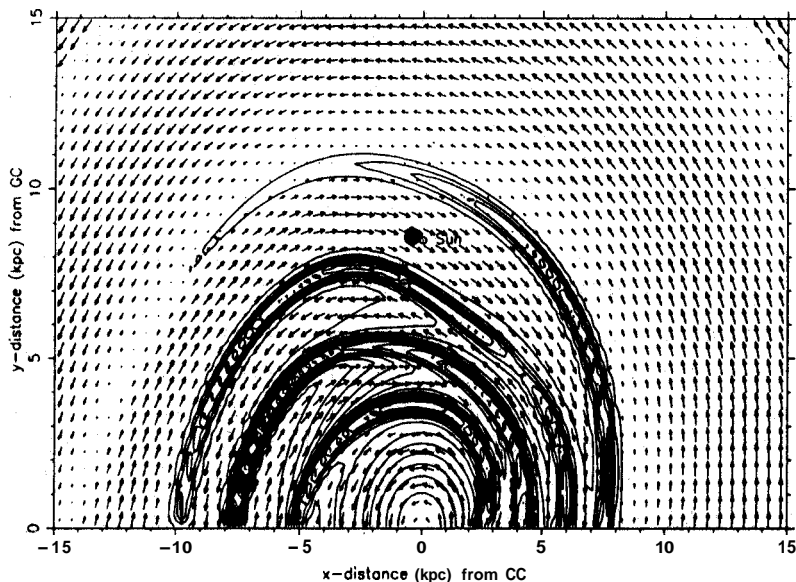


Figure 6.8: A model for the magnetic field being strong in the **interarm** regions and reversing in the arm region. The contours represent the spiral arm structure of the Galaxy and the arrows denote the direction of the magnetic field and the length of the arrow represents the magnitude of the field at that point.

6.8), it is quite striking that the **magnetic** 'arms' more or less **follow** the spiral arms, but the field is stronger more often in the **interarm** regions than in the arms. While BSS model seems to be preferred (on the basis of  $\chi^2$ ) compared to the circular field model, both these models seem to have a common underlying preference for stronger fields in the **interarm** region rather than in the arm regions. This conclusion is also supported by the fact that our explicit model for fields along the spiral arms performs very poorly in comparison with magnetic field stronger in the **interarm** regions. Such a configuration is already reported in the case of one of the external galaxies NGC 6946. Linearly **polarised** radio emission from this galaxy shows two magnetic spiral arms in between the optical spiral arms. This has been interpreted as the absence of field tangling and small **Faraday** depolarisation in the **interarm** region compared to the field tangling which occur in the optical spiral arms owing to supernova explosions and turbulent motions of gas clouds (Beck & Hoernes 1996).

It is important to note the following differences between our analysis and the earlier ones. We have taken the distance of the Sun from the galactic centre as 8.5 kpc (adopted as the IAU standard), whereas earlier groups have assumed it to be 10 kpc. The effect of this is relatively minor, only some parameters such as the distance,  $d$ , to the first field reversal and the spacing between the reversals would be affected. Another, and rather **major** difference is that we have incorporated explicitly the electron density variation due to the spiral structure of our galaxy, while earlier groups have assumed the electron density

to be constant.

## 6.7 Modelling the z-component of the galactic magnetic field using extragalactic Sources

The magnetic structure in the galaxy can be revealed from the RM distribution of the extragalactic sources (ERS) **also**. The observed RM of an ERS is a linear sum of the contributions along the line of sight within the radio source itself, from the **intracluster/intergalactic** medium and from the interstellar medium of our galaxy. Based on the observed correlation between the **RMs** of the ERS and the **RMs** of pulsars **SK(1980)**, Inoue and Tabara (1981) and Vallee (1988) have argued that the **RMs** of ERS are contributed mainly by our galaxy. However, the possible large intrinsic RM **or/and** the RM contributed by **intergalactic/intracluster** medium may **cause** serious errors in the description of the galactic magnetic field based on the **RMs** of **ERS**. No clear **method** can be used to reduce or remove their influence. So all that one can do is to exclude **from** the analysis all **ERS** whose **RMs** are beyond some reasonable limit consistent with contributions from our galaxy alone.

In this section we have tried to estimate the vertical component of the local magnetic field in our galaxy. An all-sky catalogue of unambiguous **RM** values for 674 radio sources (galaxies or quasars) was compiled by Broten et al. (1988). Out of these 674 ERS, we have removed 98 ERS whose **RMs** are greater than  $300 \text{ rad m}^{-2}$  which are less likely to be produced by **the** large scale field of our galaxy. In addition to these, the ERSs behind the North Polar Spur and Gum Nebula region are also deleted from the sample used. Ultimately, there are 576 ERS available to derive the magnetic feature of our galaxy.

To determine the vertical component of the local magnetic field, **we** have taken only 103 **ERSs** whose galactic latitude is greater than or equal to  $\pm 60^\circ$ . Distribution of these **RMs** is shown in fig (6.9). It is clearly seen from this **figure** that **more positive RMs** are seen at negative latitudes and vice versa, suggesting a **possible** presence of vertical component of the magnetic field. **Han** and Qiao (1994) obtained a strength of  $0.2\text{--}0.3 \mu\text{G}$  for the vertical component by assuming constant electron density to be  $0.03 \text{ cm}^{-3}$  and the scale height for the electron distribution to be 700 pc to 1 kpc. The direction of this field points from south galactic pole to north galactic **pole**. Using a procedure similar to **that** of Han & Qiao, we estimate a value of  $0.15 \pm 0.08 \mu\text{G}$  for the vertical component of **the** magnetic field, but only after removing the contribution from the planar bisymmetric field in the galactic plane. Note that the contribution **from** the **planar component** is not negligible even while considering latitudes, within  $60^\circ - 80^\circ$ . But the  $\chi^2 = 20.3$  is hardly different from  $\chi_0^2 = 24.2$ . This may be due to the scatter of the **RMs** being large compared to the contribution due to the vertical and planar components of the galactic field. The value of  $0.15 \pm 0.08 \mu\text{G}$  for the vertical **component** suggested by this analysis should be compared with  $0.23 \mu\text{G}$  from our analysis of the pulsar data and with that derived by **Han** & Qiao ( $0.2\text{--}0.3 \mu\text{G}$ ).

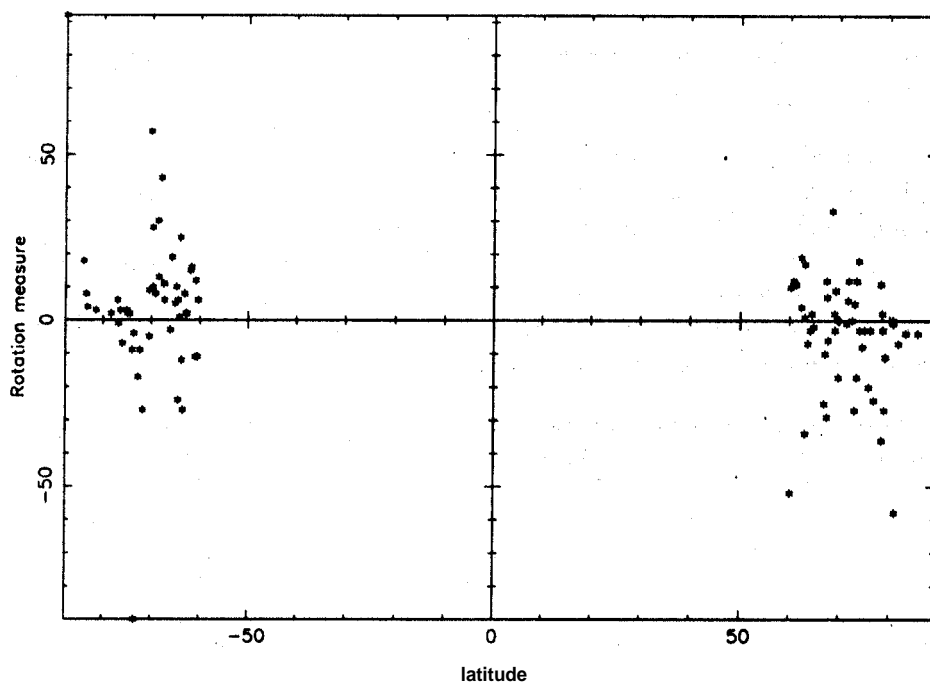


**Figure 6.9:** Distribution of the Rotation Measure of the Extragalactic Radio sources with galactic latitude  $b > 60^\circ$ . It is quite clear that positive RMs dominate the southern galaxy and vice versa.

---

## 6.8 Summary

We have examined several models for the large scale magnetic field in our galaxy using rotation measures of pulsars. We have used the model by **Taylor-Cordes** for the electron **density** variation due to the spiral structure in our galaxy. We find that

- the pulsar rotation measure data favours the Bisymmetric Spiral configuration for the large scale field over the Circular configuration.
- the bisymmetric field has strength of  $2.3 \mu\text{G}$ , pitch angle ( $p$ ) of  $6^\circ.8$  and a **galacto-**centric distance at the first maximum  $r_0 = 9.3$  kpc.
- the vertical component of the magnetic field (in the solar vicinity) is estimated to be  $\sim 0.2\mu\text{G}$ , an order of magnitude smaller compared to the large scale planar field.
- the strength of the vertical ( $z$ -) component of the magnetic field estimated from the **Faraday** rotation measures of extragalactic sources is quite consistent with the strength obtained from pulsar rotation measures.
- the best-fit bisymmetric spiral field configuration (refer fig 6.7 ) (as well as the circular ring model) shows that in most of the regions the field is stronger in the **interarm** regions rather than in the spiral arms.
- the **model** for large scale magnetic field being positively correlated with the electron density can be rejected with high confidence based on the **pulsar** RM data.

## References

- Alpar M. A., Anderson P. W., Pines D. & Shaham J., 1984a, *ApJ*, 276, 325  
Alpar M. A., Anderson P. W., Pines D. & Shaham J., 1984b, *ApJ*, 278, 791  
Alpar M. A., Chau H. F., Cheng K. S. & Pines D., 1993, *ApJ*, 409, 345  
Alpar M. A., Chau H. F., Cheng K. S. & Pines D., 1994, *ApJ*, **427**, L29  
Alpar M. A., Nandkumar R. & Pines D., 1986, *ApJ*, 311, 197  
**Alurkar** S. K., Slee O. B. & Bobra A. D., 1986, *AJP*, 39,433  
Anderson P. W & **Itoh** N., 1975, *Nature*, 256, 25  
Andreasyan R. R. & **Makarov** A. N., 1989, *Afz* **31(2)**, 247  
Anish Roshi. D, 1996, **M.Sc.** Thesis, University of Pune  
Arzoumanian Z., Nice D. J. & Taylor J. H., 1994, *ApJ*, 422, 671  
**Baade** W. & Zwicky F., 1934, "Supernovae", *Proc. natn. Acad. Sci., U.S.A.*,  
20, 254  
Backer D. C., 1989, "Pulsars" in Galactic and Extragalactic *radio* astronomy, eds.  
Verschuur G. L. & Kellerman K. I., pp 480-551, Springer-Verlag Inc.,  
New York  
Backer D. C. & **Hellings** R. W., 1986, *ARAA*, 24, 537  
Backer D. C. & **Rankin** J. M., 1980, *ApJS*, 42, 143  
Baym G., **Pethick** C., Pines D. & Ruderman M. A., 1969, *Nature*, 224, 872  
Beck R. & Hoernes P., 1996, *Nature*, 379, 47  
Blandford R. D., **Hewish** A., Lyne A. G. & **Mestel** L., 1992, Pulsars as physics  
Laboratories, *Phil. Trans. R. Soc. Lond. A.*, 341, pp. 1-192  
Blandford R. D., **Narayan** R. & **Romani** R. W., 1984, *JAA*, 5, 369  
Blandford R. D. & Teukolsky S.A., 1976, *ApJ*, 205, 580  
**Bolton** J. G. & Wild J. P., 1957, *ApJ*, 125, 296  
Boynton P. E. & **Deeter** J. E., 1986, preprint  
Boynton P. E., Groth E. J., Hutchinson D. P., Nanos G. P., Partridge R. B.  
& Wilkinson D. T., 1972, *ApJ*, 175, 217.  
Brandenburg A., Krause F., **Meinel** R., Moss D. & **Tuominen** I., 1989, *A&A*,  
213, 41  
Brotten N. W., **MacLeod** J. M. & Vallee J. P., 1988, *Ap&SS*, 141, 303  
Buczlowski U. R., 1985, **PhD** thesis, Univ. Bonn, West Germany

- Cheng K. S., 1987a, *ApJ*, 321, 799
- Cheng K. S., 1987b, *ApJ*, 321, 805
- Cheng K. S., 1989, "A model of pulsar timing noise", in *Timing Neutron Stars*, eds. Ögelman H. & van den Heuvel E. P. J., pp. 503-509, **Kluwer Academic Publishers, Dordrecht**
- Cheng A. F. & Ruderman M. A., 1979, *ApJ*, 229, 348
- Chi X. & Wolfendale A. W., 1990, *J. Phys. G. Nucl. Part. Phys.* 16, 1409
- Cordes J. M., 1993, "The detectability of planetary companions to radio pulsars" in *Planets around Pulsars*, pp. 43-60, **Astronomical Society of the Pacific, San Francisco**
- Cordes J. M. & Downs G. S., 1985, *ApJS*, 59, 343
- Cordes J. M., Downs G. S. & Krause-Polstorff J., 1988, *ApJ*, 330, 847
- Cordes J. M. & Greenstein J. L., 1981, *ApJ*, 245, 1060
- Cordes J. M. & Helfand D. J., 1980, *ApJ*, 239, 640
- D'Alessandro F., 1995, **Ph.D.** Thesis, University of Tasmania
- Davis L. & Greenstein J. L., 1951, *ApJ*, 114, 206
- Deshpande A. A. & McCulloch P., 1993, Preprint
- Deshpande A. A., Ramachandran R. & Srinivasan G., 1995, *JAA*, 16, 53
- Downs G. S., 1982, *ApJ*, 257, L67
- Downs G. S. & Reichley P. E., 1983, *ApJS*, 53, 169
- Drake F. D. & Craft H. D., 1968, *Nature*, 220, 231
- Fujimoto M., Kawabata K. & Sofue Y., 1971, *Prog. Theor. Phys. Suppl.* 49, 181
- Ginzburg V. L. & Syrovatskii S. I., 1969, *ARAA*, 7, 375
- Gold T., 1968, *Nature*, 218, 731
- Goldreich P. & Julian W. H., 1969, *ApJ*, 157, 869
- Greenstein J. L., 1979a, *Nature*, 277, 521
- Greenstein J. L., 1979b, *ApJ*, 231, 880
- Greenstein J. L., 1981, "Glitches, timing noise, and pulsar thermometry" in *Pulsars*, IAU symposium no. 95, eds. Sieber W. & Wielebinski R., pp. 291-298, **Riedel, Dordrecht**
- Groth E. J., 1975a, *ApJS*, 29, 443
- Groth E. J., 1975b, *ApJS*, 29, 453
- Gullahorn G. E. & Rankin J., 1978, *AJ*, 83, 121
- Gwinn C. R., Bartel N. & Cordes J. M., 1993, *ApJ*, 410, 673
- Hall J. S., 1949, *Science*, 109, 166
- Han J. L., Manchester R. N., Berkhuysen E. M. & Beck R., 1996, Preprint
- Han J. L., & Qiao G. J., 1994, *A&A*, 288, 759
- Hankins T. H., 1971, *ApJ*, 169, 487
- Hankins T. H., 1972, *ApJ Lett.*, 177, L11
- Hankins T. H. & Rickett B. J., 1975, "Pulsar signal processing", in *Methods in Computational physics*, eds. Alder B., Fernbach S. & Rotenberg M., 14,

- pp. 56–129, Academic Press, New York
- Harding** A. K., Shinbrot T. & **Cordes** J. M., 1990, *ApJ*, 353, 588
- Harrison P. A., Lyne A. G. & Anderson B., 1993, *MNRAS*, 261, 113
- Haynes R. F., Stewart R. T., Gray A. D., **Reich** W., Reich P. & **Mebold** U., 1992, *A&A*, 264, 500
- Hewish** A., Bell S. J., Pillington J. D. H., Scott P. F. & Collins R. A., 1968, *Nature*, 217, 709
- Hiltner W. A., 1949, *Science*, 109, 165
- Hiltner W. A., 1958, *ApJ*, 128, 9
- Horellou C., Beck R. & **Berkhuijsen** E. M., 1992, *AA*, 265, 417
- Inoue M. & **Tabara** H., 1981, *PASJ*, 33, 603
- Jahan** Miri, 1996, **Ph.D.** Thesis, Indian Institute of Science
- Jones P. B., 1990, *MNRAS*, 246, 364
- Kapahi** V. K., **Damle** S. H., Balasubramanian V. & Swarup G., 1975, *J. IETE*, 31, 117
- Kaspi V. M., Taylor J. H. & Ryba M. F., 1994, *ApJ*, 428, 713
- Komaseroff M. N., 1970, *Nature*, 226, 612
- Krause M., **Beck** R. & Hummel E., 1989b, *A&A*, 217, 17
- Krause M., **Hummel** E. & **Beck** R., 1989a, *A&A*, 217, 4
- Kronberg P. P., 1994, *Rep. Prog. Phys.* 57, 325
- Large M. I., **Vaughan** A. E. & Mills B. Y., 1968, *Nature*, 220, 340
- Lamb F. K., 1981, "Neutron star properties from observations of pulsars and pulsing X-ray sources" in *Pulsars*, IAU symposium no. 95, eds. Sieber W. & **Wielebinski** R., pp.303–319, **Riedel, Dordrecht**
- Lamb F. K., Pines D. & **Shaham** J., 1978a, *ApJ*, 224, 969
- Lamb F. K., Pines D. & **Shaham** J., 1978b, *ApJ*, 225, 582
- Lyne A. G., 1987, *Nature*, 326, 569
- Lyne A. G., Anderson B. & Salter M. J., 1982, *MNRAS*, 201, 503
- Lyne A. G. & Manchester R. N., 1988, *MNRAS*, 234, 477
- Lyne A. G., **Manchester** R. N. & Taylor J. H., 1985, *MNRAS*, 213, 533
- Lyne A. G., Pritchard R. S. & Smith F. G., 1993, *MNRAS*, 265, 1003
- Lyne A. G., Pritchard R. S. & **Shemar** S. L., 1994, *JAA*, 16, 179
- Lyne A. G. & Smith F. G., 1989, *MNRAS*, 237, 533
- Lyne A. G. & Smith F. G., 1990, *Pulsar Astronomy*, Cambridge University, Cambridge
- McCulloch P. M., Hamilton P. A., **McConnell** D. & King E. A., 1990, *Nature*, 346, 822
- McCulloch P. M., Hamilton P. A., **Royle** G. W. R. & Manchester R. N., 1983, *Nature*, 302, 319
- McCulloch P. M., Klekociuk A. R., Hamilton P. A. & **Royle** G. W. R., 1987, *ApJ*, 40, 725

- Manchester R. N., 1974, **ApJ**, 188, 637  
 Manchester R. N. & Taylor J. H., 1977, Pulsars, **W.H.Freeman & Co., San Francisco**  
 Mansfield V. N. & **Rankin J.**, 1977, *Vistas in Astronomy*; 21, 393  
 Mathewson D. S. & Ford V. L., 1970, *Mem. R. Astron. Soc.*, 74, 139  
 Mathewson D. S., **van der Kruit P. C.** & Brouw W. N., 1972, **A&A**, 17,468  
 Morris D. & Berge G. L., 1964, **ApJ**, 139, 1388  
 Muliarchik T. M., 1957, **Izvest. Astrophys. Inst. Alma Ata**, **5(7)**  
**Narayan R.** & **Ostriker J. P.**, 1990, **ApJ**, 352, 222  
**Ohman Y.**, 1942, *Stockholm Obs. Ann.* **14(4)**, 1  
 Pacholczyk A. G., 1970, *Radio Astrophysics*, **Freeman, San Francisco**  
 Pacini F., 1967, *Nature*, 216, 567  
 Pacini F. & Rees M. J., 1970, *Nature*, 226, 622  
 Parker E. N., 1971, **ApJ**, 163, 252  
 Parker E. N., 1979, **Cosmical Magnetic Fields**, pp. **795-819**, oxford, Clarendon  
 Phinney E. S. & **Blandford R. D.**, 1981, *MNRAS*, 194, 137  
 Piddington J. H., 1964, *MNRAS*, **128**, 345  
 Piddington J. H., 1978, *Astrophys. Space Sci.*, 59, 237  
 Piddington J. H., 1981, *Astrophys. Space Sci.*, 80, 457  
 Pines D. & **Shaham J.**, 1972, *Nature*, 235, 43  
 Prentice A. J. R. & ter Haar D., 1969, *MNRAS*, 146,423  
**Radhakrishnan V.** & Cooke D. J., 1969, **ApJ Lett.**, 3,225  
**Ramachandran R.**, 1996, **Ph.D. Thesis, Osmania University**  
 Ramachandran R. et al., 1997, *MNRAS*, submitted  
 Ramkumar P. S., Prabu T., **Madhu Girimaji & Markandeyulu G.**, 1994, **JA&A**, 15, 343  
 Rand R. J. & **Kulkarni S. R.**, 1989, **ApJ**, 343, 483  
**Rankin J.**, 1983a, **ApJ**, 274, 333  
**Rankin J.**, 1983b, **ApJ**, 274, 359  
**Rankin J.**, 1986, **ApJ**, 301, 901  
**Rankin J.**, 1990, **ApJ**, **352**, 247  
**Rankin J.**, 1993, **ApJ**, 405, 285  
**Rickard J. J.** & Cronyn W. M., 1979, **ApJ**, 228, 755  
 Rickett B. J., 1977, *ARAA*, 15, 479  
 Rickett B. J., 1990, *ARAA*, 28, 561  
 Rickett B. J., **Coles W. A.** & Bourgois G., 1984, **A&A**, 134, 390  
 Ritching R. T., 1976, **MNRAS**, 176, 249  
 Ruderman M. A., 1969, *Nature*, 233, 597  
 Ruderman M. A., 1970, *Nature*, 225, 619  
 Ruderman M. A., 1970, *Nature*, 225, 838  
 Ruderman M. A. & Sutherland P. G., 1975, **ApJ**, 196, 51  
**Ruzmaikin A. A.**, Sokolov D. D. & **Shukurov A. M.**, 1985, **A&A**, 148, 335

- Ryba M. F. & Taylor J. H., 1991, **ApJ**, **371**, 739
- Salter C. J., 1983, Bull. Astr. Soc. India, **11**, 1
- Sarma N. V. G., Joshi M. N. & Ananthakrishnan S., **1975b**, J. IETE, **21**, 107
- Sarma N. V. G., Joshi M. N., Bagri D. S., & Ananthakrishnan S., **1975a**,  
J. IETE, **21**, 110
- Sawa T. & Fujimoto M., 1986, PASJ, **38**, 133
- Scarrot** S. M., White C., Pallister W.S. & **Solinger** A. B., 1977, Nature, **266**, 32
- Scheuer P. A. G., 1968, Nature, **218**, 920
- Shapiro I. I., 1964, PRL, **13**, 789
- Shklovsky I. S., 1970, **ApJ** Lett., **8**, 101
- Simard-Normandin** M. & Kronberg P. P., 1980, **ApJ**, **242**, 74
- Smith F. G., 1977, *Pulsars*, Cambridge University Press, Cambridge
- Sofue Y. & **Fujimoto** M., 1983, **ApJ**, **265**, 722
- Sofue Y., Fujimoto M. & Kawabata K., 1979, Publ. Astron. Soc. Jpn., **31**, 125
- Sofue Y., Fujimoto M., & Wielebinski R., 1986, ARAA, **24**, 459
- Sofue Y., Klein U., **Beck** R. & Wielebinski R., 1985, **A&A**, **144**, 257
- Sofue Y., **Takano** T. & Fujimoto M., 1980, **A&A**, **91**, 335
- Staelin D. H. & **Reifenstein** E. C., 1968, Science, **162**, 1481
- Standish** E.M., 1982, **A&A**, **114**, 297
- Stinebring D. R. & **Cordes** J. M., 1990, **ApJ**, **362**, 207
- Strachenko** S. V. & **Shukurov** A. M., 1989, **A&A**, **214**, 47
- Sturrock P. A., 1971, **ApJ**, **164**, 529
- Sutton J. M., 1971, MNRAS, **165**, 51
- Swarup** G., Sarma N. V. G., Joshi M. N., Kapahi V. K., Bagri D. S., **Damle** S. H.,  
Ananthakrishnan S., **Balasubramanian** V., Bhave S. S. & **Sinha** R. P., 1971,  
Nature Phys. Science, **230**, 185
- Taylor J. H., 1991, Proceedings of the IEEE, **79**, 1054
- Taylor J. H. & **Cordes** J. M., 1993, **ApJ**, **411**, 674
- Taylor J. H., **Manchester** R. N. & Lyne A. G., 1993, **ApJS**, **88**, 529
- Taylor J. H. & **Stinebring** D. R., 1986, ARAA, **24**, 285
- Taylor J. H. & **Weisberg** J., 1989, **ApJ**, **346**, 434
- Taylor J. H., **Wolszczan** A., **Damour** T. & **Weisberg** J. M., 1992, Nature, **355**, 132
- Taylor J. H. et al., 1975, **ApJ**, **196**, 513
- Thomson R. C., Nelson A. H., 1980, MNRAS, **191**, 863
- Tosa M. & Fujimoto M., 1978, Publ. Astron. Soc. Japan, **30**, 315
- Vallee J. P., 1984, AA, **136**, 373
- Vallee** J. P., 1988, AJ, **95(3)**, 750
- Vallee J. P., 1991, **ApJ**, **366**, 450
- Vallee J. P., 1995, **ApJ**, **454**, 119
- Vivekanand & **Narayan** R., 1981, JAA, **2**, 315
- Weller G. L., Perry J. J. & Kronberg P. P., 1984, **ApJ**, **279**, 19
- Wolszczan A. & Frail D. A., 1992, Nature, **355**, 145

- Wolszczan A., 1993, "PSR 1257+12 and its planetary companions", in *Planets around Pulsars*, pp.3-10, Astronomical Society of the Pacific, San Francisco
- Wolszczan A., 1994, *Astrophys. Sp. Sci.*, **212**, 67
- Yusef-Zadeh F. & Morris M., 1987, *AJ*, **94**, 1178